NUMERICAL ASSESSMENT AND VALIDATION OF THE ENERGY-BASED VARIATIONAL APPROACH TO COUPLED THERMO-MECHANICAL PROBLEMS

A thesis submitted in partial fulfillment for the degree of:

Master of Science in Computational Mechanics

by

Shabeer Khan

Supervisor:
Prof. Laurent STAINIER
Ecole Centrale de Nantes - Institut GeM (UMR 6183 CNRS)

Nantes, 16^{th} June, 2011

Ecole Centrale de Nantes,France
Institut GeM (UMR 6183 CNRS)

Preface

The thesis is submitted in partial fulfillment of requirements for the Degree of Master of Science in Computational Mechanics. It contains the work started from September, 2010 to February, 2011. The work is carried under consistent supervision of Prof. Dr. Laurent STAINIER, from Ecole Centrale de Nantes and Institute GeM, France. Tasks for the thesis have been achieved during the mentioned period in the laboratories of the *Ecole Centrale de Nantes, France*.

The thesis report is tried to be written in a very simple and effective manner. Even though the topic is much complicated and advanced in respect of multidisciplinary studies of mechanics and thermodynamics, but the bearer tried to make it clear and specific, with the help of easily comprehendible governing equations and suitable examples. It is assured that the required results are discovered and most of the important topics are described to the best of bearer. Moreover, useful references are cited at required places.

For further information please contact:
Shabeer Khan: engr.s.khan@gmail.com
The supervisor can be contacted at:
Prof. Dr. STAINIER, L. stainier.Laurent@ec-nantes.fr

Disclaimer

The thesis work was carried out at Ecole Centrale de Nantes & LPC Research Laboratories, Nantes, France under the supervision of Prof. Laurent STAINIER from ECN and GeM Institut CNRS. The thesis was completed in 6 months from September, 2010 till February, 2011.

I hereby declare that this thesis is entirely the result of my own work and I have taken the required permission wherever it is necessary. I have used only the resources given in the list of references. The whole work is my own interpretation, I hereby agree to indemnify and save harmless my supervisors from any and all claims which may be asserted or which may arise.

Shabeer Khan

Signature:.....

Date:.....

Place:.....

Acknowledgement

I am grateful to thank my supervisor *Prof. Laurent STAINIER* from Institut GeM (Civil and Mechanical Structural Research Centre) Ecole Centrale de Nantes. I am indebted to him for introducing me to this topic. He has helped me at all stages of the thesis work right from providing reference material to proofreading the thesis report. This thesis would not have been possible without immense support of him. Apart from guiding me, he has introduced me to to the effective way of scientific thinking approach and help me built my confidence with the humble way of cooperation. I am delighted to work with him and really appreciate the support and generosity during all the period.

It is pleasure for me to thank the IT personals for letting me use the computing machines comfortably and helping me whenever I needed them for any technical assistance. It would be unfair not to mention the name of Eric MANCEAU and many thanks for his cooperation.

Working as an Erasmus Mundus scholar, it was very nice period of my life. It was my pleasure to have the label of Excellence in the form of European Union Erasmus Mundus. I am grateful for providing me such an innovative environment and prestigious awards by European Union.

Last but not least, I would like to thanks to the colleagues, *Fabien, Santiago and Feifei*, who were in the same department and in the same course. They have created convivial atmosphere at work place and were always nice to me in their own way of discussion and amusement.

Before I wind up my words, I offer my regards and blessings to all of those who helped me in any respect during the completion of the thesis by their illustrious support. Although I do not have sufficient words to thank them, yet I make this endeavor to express my gratitude for them.

Shabeer Khan

Abstract

The coupled thermo-mechanical problems in solid mechanics are the deformable solids, possibly undergoing a large deformations, possessing viscosity, internal processes and capable of conducting heat. Problems of such a nature arises in variety of important fields of applications, including; metal forming, machining, casting and other manufacturing processes, high velocity impact such as ballistic penetration, and many others. The variational form of such problems mean a functional satisfying all the energy, momentum and entropy equations and whose stationary points are the solution of such problems. The coupled thermo-mechanical problems usually consists of a deformable, inelastic and dissipative solid with heat conduction. The variational formulation of the coupled thermo-mechanical boundary value problem for general dissipative solids is investigated by considering a specific example of necking problem and the results are then compared with academic code and commercial code.

The energy based variational formulation is used for the general dissipative solids, including finite elastic and plastic deformations, non-Newtonian viscosity, rate sensitivity, arbitrary flow and hardening rules, as well as heat conduction. In the recent years,the more concentration was put on finding a joint potential function such that both the energy conservation equations and linear momentum balance equations should be satisfied including amount of dissipated energy. It has been an important field from computational point of view also because of its different nature from conventional finite element method. The famous radial return mapping method was under consideration in many PhD thesis. Here in the thesis, the results of the methods used in computations for thermoplasticity are compared, and the radial return mapping method for viscoplasticity is also investigated. The effect of change of flow criteria with respect to temperature due to the evolution of plastic entropy are discussed along the J_2 flow theory and the incompressibility constraints on plastic flow. The model incorporating the multiplicative decomposition of deformation gradient into elastic and plastic parts, as in the phenomenological models described by Lee and Mandel as well as the micromechanical models of single crystal plasticity inspired in the classical Taylor, Simo and Miehe models are investigated along the progression of work. The models by *Simo and Miehe, 1992*[13], *Marko Canadijia and Josip Brnic, 2003*[29], and *P. Wriggers et al., 1991*[16] are discussed in detailed to give the complete idea of balance equations, governing equations, constitutive equations, and evolution equations with reference to J_2 flow theory.

Here in the mentioned thesis, few of the constitutive models of solid mechanics are tried to be explained along with their computational solution methods. These constitutive models are narrated completely in the sense that what is meant by the solution of problem, what sort of values are given, what are the governing equations, what is the new in the governing equation as compared to the previous one, what are the new developments in such models, what is the numerical methods adopted for formulating such models and what is the main point of focus in the current model during numerical simulation by comparing with the last model. The constitutive models are started from the simplest one, which is static linear elastic model,hyperelasticity and viscoplasticity. The computational part of the thesis is presented in the part II, which is the comparison for different varying parameters of academic code and Abaqus simulations for necking problem, e.g. change of temperature, mesh sizes, integration types, effect of convection heat coefficient, variation of time step of load application, and many other parameters. Different types of mesh are used for the same geometry, the classical necking problem. The load, displacements, temperature, strains and stresses are computed and compared with the academic code which is coded by Prof. Dr. Laurent Stainier in the Intitute-Gem Ecole Centrale de Nantes, France.

Contents

List of Figures

Part I

Theory: Models for Coupled Thermo-visco-plasticity

Chapter 1

Basic Laws of Mechanics and Thermodynamics

It is well understood that the thermomechanical response of the solid undergoing plastic deformation is governed by the balance of a linear momentum equaion and the energy equations, supplemented by the constitutive equations along the appropriate boundary conditions. All these basic laws are defined in terms of continuum.There are always two ways of observing these laws with respect to time and position, and two ways of writing it.These two ways of observation are called, Lagrangian Form and Eulerian form. Lagrangian form always observe the thing with respect to reference confuguation (and is mostly used in solid mechanics, because we need reference configuration to observe the deformed state of solid) and the Eulerian form observe the things in the current configurations (and is mostly used in fluids, because in fluids we do not need the reference configuration as much). All these laws are explained here briefly.

Theorem 1 Reynold's Theorem: *The Reynold Theorem refers to any extensive property of the fluid in a particular control volume. It is expressed with the material derivative on left side, as;*

$$\frac{DN_{sys}}{Dt} = \int_{c.v} \frac{\partial}{\partial t}(\rho\eta)dV + \int_{c.s} \rho\eta\vec{v}_b \cdot \hat{n}dA + \int_{c.s} \rho\eta\vec{v}_r \cdot \hat{n}dA \tag{1.1}$$

Theorem 2 Green's Theorem: *The Green theorem is the vector identity and is equivalent to curl theorem in plane. It states that line integral for closed path can be written as a surface integral as;*

$$\int_{\partial D} f(x,y)dx + g(x,y)dy = \int\int_{D} \Big(\frac{\partial f}{\partial x} - \frac{\partial g}{\partial y}\Big)dxdy \tag{1.2}$$

1.1 Conservation of Mass

The conservation of mass is always the change of density with respect to position and time, or in other words, the time derivative of the density with respect to time and position. It

should always be zero in order to satsify the law of conservation of mass in solid mechanics. Balance of the mass is enforced at the outset merely by requiring , where is the reference density, and the balance of angular momentum reduces to the symmetry condition, it is also enforced at the outset. Expressing the differential form of mass conservation in Eulerian form gives the Continuity equation and the integral form of mass conservation equation helps in derivation of Reynold's Transport theorem. The differential and integral form of mass conservation equation are shown below both for Lagrangian and Eulerian form respectively.

$$\frac{\partial \boldsymbol{\rho_{ij}}}{\partial t} = 0 \tag{1.3a}$$

$$\int_{\mathrm{V}} \boldsymbol{\rho(x,t)} dV = 0 \tag{1.3b}$$

$$\frac{\partial \boldsymbol{\rho_{ij}}}{\partial t} + \nabla(\boldsymbol{\rho v}) = 0 \tag{1.3c}$$

$$\int_{\mathrm{V}} [\dot{\boldsymbol{\rho}}\boldsymbol{(x,t)} + \boldsymbol{\rho(x,t)} \nabla \boldsymbol{v}] = 0 \tag{1.3d}$$

1.2 Conservation of Momentum

This is the newton law of momentum. It says that the rate change of momentum (due to body forces and traction forces) is equal to the change of force. Using the Green Theorem we get the following integral and differential forms of Newton's Law of momentum (F=ma).

$$\int_{\mathrm{V}} \rho \dot{\boldsymbol{v}} dv = \int_{\partial \mathrm{V}} \rho \boldsymbol{b} dv + \int_{\mathrm{V}} \boldsymbol{t} d\mathrm{A} \tag{1.4a}$$

$$\int_{\mathrm{V}} \rho \dot{\boldsymbol{v}} dv = \int_{\partial \mathrm{V}} \rho \boldsymbol{b} dv + \int_{\mathrm{V}} \boldsymbol{\sigma} \cdot \boldsymbol{n} d\mathrm{A} \tag{1.4b}$$

$$\rho \dot{\boldsymbol{v}} = \rho \boldsymbol{b} + \boldsymbol{\nabla} \cdot \boldsymbol{\sigma} \tag{1.4c}$$

Similarly by multiplying with velocity, we get the angular momentum balance.

1.3 First Law of Thermodynamic

The first law of thermodynamics is simply the conservation of energy, that energy can never be created and can never be destroyed, but it just can be changed from one state to another. In simplest way, it states that the change in energy (internal energy and kinetic energy) of the system is equal to the heat supplied minus the work done by the system on the surrounding, or the heat supplied to a system is equal to the change in internal energy of the system and the work done by system, e.g. if one supply a heat to the glass of water, then that heat will

be there in the form of change of internal energy and the work of thermal expansion of glass, and it will remain forever if one consider there is no sink.

$$\begin{aligned} dU &= \delta Q - \delta W \\ \delta Q &= dU + \delta W \end{aligned} \tag{1.5}$$

If the work is also done on the body (usually in mechanics), then the change in the energy of the body is equal to heat supplied and the work done on the system, i.e. change in power of system (internal power)should be equal to the power supplied by the surrounding (external power). In the other words, the external power and heat supplied is equal to change in kinetic energy of the body and the internal energy of the body.

$$\begin{aligned} dU &= \delta Q + \delta W \\ \dot{\kappa} + \dot{u} &= \dot{Q} + \dot{W} \end{aligned} \tag{1.6}$$

Putting the kinetic energy and internal energy of the body (after using Reynold's Transport Theorem),heat supplied and external power (after using the Green Theorem), we get the following differential form of the energy balance equation.

$$\rho \dot{\boldsymbol{u}} = \boldsymbol{\sigma} : \nabla \boldsymbol{v} + \rho r - \nabla \cdot \boldsymbol{q} \tag{1.7}$$

Having the symmetry of $\boldsymbol{\sigma}$, we get the following differential equation of energy in Eulerian form.

$$\rho \dot{\boldsymbol{u}} = \boldsymbol{\sigma} : \boldsymbol{D} + \rho r - \nabla \cdot \boldsymbol{q} \tag{1.8}$$

where $\boldsymbol{D}$ is the symmetric part of the velocity gradient, $\nabla \boldsymbol{v}$.

1.4 Second Law of Thermodynamic

The second law of thermodynamics explain the relation of two state variables, temperature and entropy. The second law of thermodynamics says that the net entropy generated by the system should always be positive, in other words, the order of the internal fineness of the system can never be refined further, it is always disturbed whenever we activate some process on it, and this disturbance is termed as entropy generation. If we (surrounding) do some work or supply heat to the body (system), so it only disturb the fineness and generates the entropy. In other words, one cay say that the difference between the entropy supplied to the body and the entropy contained by the body can be either zero or positive number, it can never be a negative number.

$$S_b - S_e \geq 0 \tag{1.9}$$

Where S_b and S_e are given as:

$$S_b = \int_V \boldsymbol{\rho \eta}(x,t) dV \qquad \textit{(entropy of the body)} \tag{1.10}$$

$$S_e = \int_V \frac{\boldsymbol{\rho} r}{\boldsymbol{\theta}} - \int_{\partial V} \frac{\boldsymbol{q} \cdot \boldsymbol{n}}{\boldsymbol{\theta}} dS \qquad \textit{(entropy from external sources)} \tag{1.11}$$

Using the Reynold's theorem and Divergence theorem, we get the renowned form of Second Law of Thermodynamics

$$\int_V \left[\boldsymbol{\rho} \dot{\boldsymbol{\eta}} - \frac{\boldsymbol{\rho} r}{\boldsymbol{\theta}} + \nabla \cdot \left(\frac{\boldsymbol{q}}{\boldsymbol{\theta}} \right) dV \right] \geq 0 \tag{1.12}$$

Solving futher and writing in the differential form, we get the Clausius Duhem Inequality.

$$\boldsymbol{\theta} \dot{\boldsymbol{\gamma}} = \boldsymbol{\rho} \boldsymbol{\theta} \dot{\boldsymbol{\eta}} - \boldsymbol{\rho} r + \nabla \cdot \boldsymbol{q} - \frac{1}{\boldsymbol{\theta}} \boldsymbol{q} \cdot \nabla \boldsymbol{\theta} \geq 0 \tag{1.13}$$

From first law of thermodynamics, putting the value of $\boldsymbol{\rho} r$, we get the following relation.

$$\boldsymbol{\theta} \dot{\boldsymbol{\gamma}} = \underbrace{\boldsymbol{\sigma} : \boldsymbol{D} - \rho \dot{\boldsymbol{u}} + \quad \boldsymbol{\rho} \boldsymbol{\theta} \dot{\boldsymbol{\eta}}}_{\textit{Internal Dissipation}} \quad - \quad \underbrace{\frac{1}{\boldsymbol{\theta}} \boldsymbol{q} \cdot \nabla \boldsymbol{\theta}}_{\textit{External Dissipation}} \quad \geq 0 \tag{1.14}$$

The Helmholtz Free Energy function is always obtained by subtracting the $\boldsymbol{\eta\theta}$ from the internal energy of the body.

$$\begin{aligned} \boldsymbol{\psi} &= \boldsymbol{u} - \boldsymbol{\eta} \boldsymbol{\theta} \\ \dot{\boldsymbol{\psi}} &= \dot{\boldsymbol{u}} - \dot{\boldsymbol{\eta}} \boldsymbol{\theta} - \boldsymbol{\eta} \dot{\boldsymbol{\theta}} \end{aligned} \tag{1.15}$$

Therefore the Clausius Duhem Inequality in the form of Helmholtz Free Energy Function can be written in the following form.

$$\boldsymbol{\theta} \dot{\boldsymbol{\gamma}} = \boldsymbol{\sigma} : \boldsymbol{D} - \boldsymbol{\rho} \dot{\boldsymbol{\psi}} - \boldsymbol{\rho} \dot{\boldsymbol{\theta}} \boldsymbol{\eta} - \frac{1}{\boldsymbol{\theta}} \boldsymbol{q} \cdot \nabla \boldsymbol{\theta} \geq 0 \tag{1.16}$$

1.5 Strain Energy Density

It is a measure of the energy stored by the strains produced within the system. It is defined as;

$$U(\varepsilon) = \int_0^{\varepsilon} \boldsymbol{\sigma} : d\varepsilon \tag{1.17}$$

If the strain energy density is path independent then, the $U(\varepsilon)$ acts as potential for stress.

$$\boldsymbol{\sigma} = \frac{\partial U(\varepsilon)}{\partial \varepsilon_{ij}} \tag{1.18}$$

In perfect elasticity, for adiabatic process, $U(\varepsilon)$ is the change in internal energy per unit volume and for isothermal process, it is the change in Helmholtz free energy per unit volume.

1.6 Principle of Virtual Work

It states that if the stress field σ_{ij} satisfy the following equation

$$\int_R \sigma_{ij}\delta\varepsilon_{ij}dV_o - \int_R b_i\delta v_i dV_o - \int_{\partial_2 R} t_i\delta v_i dA = 0 \tag{1.19}$$

where $\delta\varepsilon_{ij} = 1/2(\partial\delta v_i/\partial x_j + \partial u_j/\partial x_i)$, for all possible virtual displacements and strains, then it will automatically satisfy the stress equilibrium equation $\partial\sigma_{ij}/\partial x_i + b_j = 0$ and also traction boundary conditions $\sigma_{ij}n_i = t_j^*$ on $\partial_2 R$.

1.7 Variational Formulation

To illustrate the variational formulation, the simple governing equations of the bar will be derived from the Minimum Potential Energy principle. Here the example of bar is taken. The general procedure of handling the equations is illustrated in the tonti diagram Figure

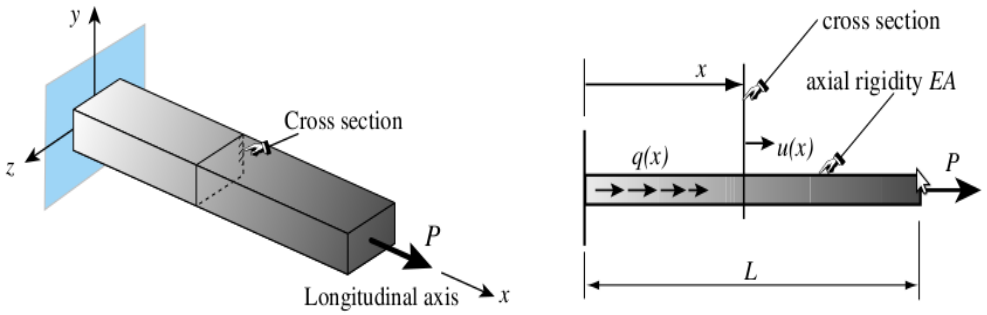

Figure 1.1: The one dimensional bar variational formulation

1.2 for the one dimensional bar example.

1.7.1 The Total Potential Energy Functional

The construction of structural and continuum finite elements using a variational formulation is based on the Total Potential Energy Principle. In a linear elastic bar, the strain energy density at one point under the stress σ and strain e is:

$$\mathcal{U} = \frac{1}{2}\sigma(x)e(x) \tag{1.20}$$

Where $\sigma = Ee$ and $e = du/dx$. Integration over the volume gives the total internal energy of the structure, which can be written as:

$$U = \frac{1}{2}\int_V \sigma e dV = \frac{1}{2}\int_0^L Fedx = \frac{1}{2}\int_0^L (EAu')u'dx = \frac{1}{2}\int_0^L u'EAu'dx \tag{1.21}$$

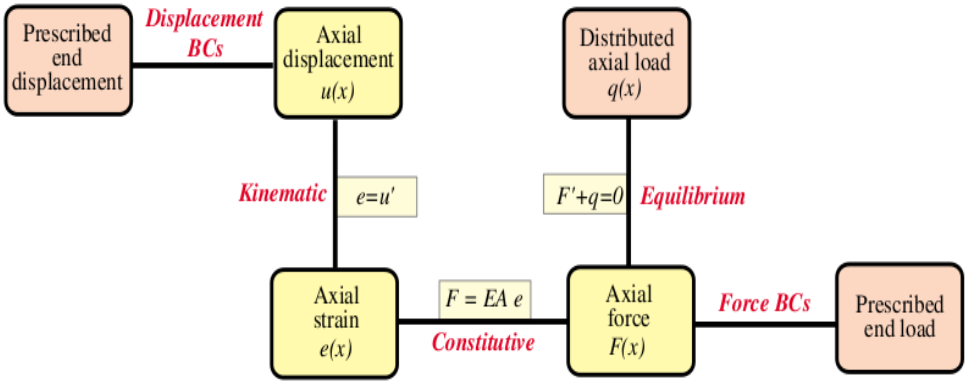

Figure 1.2: Tonti diagram for the continuum model of a bar member. Field equations and BCs are represented as lines connecting the boxes. Yellow (brown) boxes contain unknown (given) quantities.

The external energy due to applied mechanical loads is from two sources:

- The distributed load $q(x)$. This contributes a cross-section density of $q(x)u(x)$ because q is assumed to be already integrated over the section.

- Any applied end load. In case of bar (one end fixed, and one end is free)the end load P would contribute $Pu(L)$.

The second source may be folded into the first by conventionally writing any point load P acting at a cross section $x = a$ as a contribution $P\delta(a)$ to $q(x)$, where $\delta(a)$ denotes the one-dimensional Dirac delta function at $x = a$. If this is done the external energy can be concisely expressed as

$$W = \int_0^L qudx. \tag{1.22}$$

The total potential energy of the bar is given by

$$\boxed{\Pi = U - W} \tag{1.23}$$

Mathematically this is a functional, called the Total Potential Energy functional or TPE. It depends only on the axial displacement u(x) here in current case. In variational calculus this is called the primary variable of the functional. When the dependence of π on u needs to be emphasized we shall write $\Pi[u] = U[u]W[u]$, with brackets enclosing the primary variable. To display both primary and independent variables we write, for example,$\Pi[u(x)] = U[u(x)]W[u(x)]$.

1.7.2 Variation of Admissible Function

The concept of admissible variation is fundamental in both variational calculus and the variationally formulated FEM. Only the primary variable(s) of a functional may be varied. In current case, for the TPE functional, this is the axial displacement u(x).

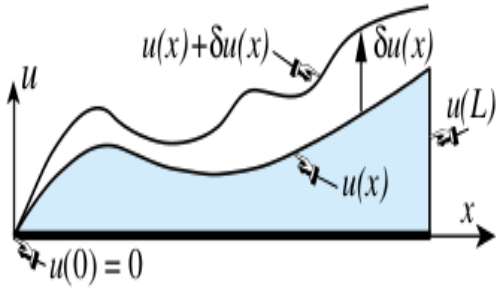

Figure 1.3: Admissibility of the variations

Suppose that u(x) is changed to $u(x) + \delta u(x)$. This is illustrated in Figure 1.3, where for convenience u(x) is plotted normal to x. The func-tional changes from Π to $\Pi + \delta\Pi$. The function $\delta u(x)$ and the scalar $\delta\Pi$ are called the variations of u(x) and Π, respectively. The variation $\delta u(x)$ should not be confused with the ordinary differential $du(x) = u(x)dx$ since on taking the variation the independent variable x is frozen; that is, $\delta x = 0$. A displacement variation $\delta u(x)$ is said to be admissible when both u(x) and $u(x) + \delta u(x)$ are kinematically admissible in the sense of the Principle of Virtual Work (PVW). This agrees with the conditions stated in the classic variational calculus.
A kinematically admissible axial displacement u(x) obeys two conditions:

- It is continuous over the bar length, that is, $u(x) \in C_0$in $x \in [0, L]$.
- It satisfies exactly any displacement boundary condition, such as the fixed-end specification, $u(0) = 0$ here in current case.

The variation u(x) depicted in Figure 1.3 is kinematically admissible because both u(x) and $u(x) + \delta u(x)$ satisfy the foregoing conditions.

1.7.3 The Minimum Potential Energy Principle

The Minimum Potential Energy (MPE) principle states that the actual displacement solution $u(x)$ that satisfies the governing equations is that which renders Π stationary:

$$\boxed{\delta\Pi = \delta U - \delta W = 0 \quad \text{iff} \quad u = u} \tag{1.24}$$

With respect to admissible variations $u = u + \delta u$ of the exact displacement field $u(x)$.

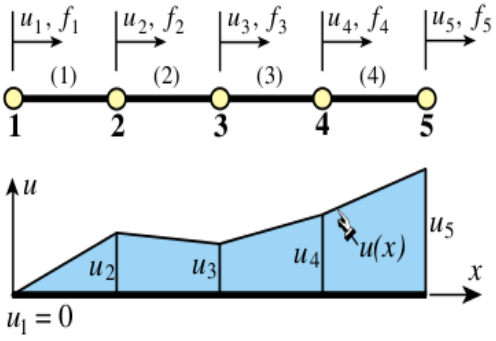

Figure 1.4: Discretization of the bar

1.7.4 TPE Discretization

To apply the TPE functional 1.23 to the derivation of finite element equations we replace the continuum mathematical model by a discrete one consisting of a union of bar elements. For example, Figure 1.4 illustrates the subdivision of a bar member into four two-node elements.

Functionals are scalars. Therefore, corresponding to a discretization such as that shown in Figure 1.4, the TPE functional 1.23 may be decomposed into a sum of contributions of individual elements:

$$\boxed{\Pi = \Pi^{(1)} + \Pi^{(2)} + ... + \Pi^{(N_e)}} \tag{1.25}$$

where N_e is the number of elements. The same decomposition applies to the internal and external energies, as well as to the stationarity condition 1.24:

$$\boxed{\delta\Pi = \delta\Pi^{(1)} + \delta\Pi^{(2)} + ... + \delta\Pi^{(N_e)} = 0} \tag{1.26}$$

Using the fundamental lemma of variational calculus,4 it can be shown that 1.26 implies that for a generic element e we may write:

$$\boxed{\delta\Pi = \delta U^e - \delta W^e} \tag{1.27}$$

This variational equation is the basis for the derivation of element stiffness equations once the displacement field has been discretized over the element, but here in the current thesis report, the rest of the finite element discretization is not carried. In mathematics the equation 1.27 is called a weak form. In mechanics it also states the Principle of Virtual Work for each element: $\delta U^e = \delta W^e$, which says that the virtual work of internal and external forces on admissible displacement variations is equal if the element is in equilibrium. *Note: The above detail on variational formulation is taken from;* www.colorado.edu/engineering/cas/courses.d/.../IFEM.Ch11.pdf by Carlos Felippa.

1.8 Overview of Constitutive Models in Plasticity

Here in the mentioned thesis, three different constitutive models of solid mechanics are explained along with their computational solution methods. The constitutive models are narrated completely in the sense that what is meant by the solution of problem, what we are given with, what are the governing equations, what is the new in the governing equation as compared to the previous one, what are the new developments in such models, what is the numerical methods adopted for formulating such models and what is the main point of focus in the current model during numerical simulation in present simulation comparing with the last model. The constitutive model will be started from the simplest one, which is static linear elastic model. Consequently, the core part of the thesis will be presented after.

- Static Linear Elasticity
- Hyperelasticity (large deformations)
- Viscoelasticity

The analytical solutions to all these problems are not well established, but some of them like for linear elastic solids and dynamic linear elastic solids are solved with Airy Stress Function Solution, Complex Variable Solution, Papkovich-Neuber Solution, and Stroth methods etc. But here in the current thesis, the variational principles based on energy and the main governing equations for some of the models are discussed briefly, and a short general FEM formulation terms are given. The mathematical forms of these terms are given in Appendix B. The model which are discussed here are linear elasticity, hyper-elasticity and visco-plasticity. The thermo-mechanical problem can be studied with any one of the above material models. The model become very complex when it becomes as rate dependent. The details of the following models can be seen from http://solidmechanics.org/contents.html by Allan F. Bower.

1.8.1 Static Linear Elasticity

Here in this section, the given values, values to be calculated, governing equations and their formulation through Principle of Virtual Work will be shortly introduced in order to get an idea about the general way of dealing problems in elasticity and plasticity.

Given Shape of the problem R, C_{ijkl} (elastic modulus), initial stresses and thermal expansion coefficients (if given), boundary conditions(displacement on $\partial_1 R$ and traction boundary condition on $\partial_2 R$).

Calculate the displacement, strain, and stress (u_i, ε_{ij},and σ_{ij}) while satisfying the following governing equations.

1. Strain-displacement equation

$$\varepsilon_{ij} = \frac{1}{2}\Big(\frac{\partial u_i}{\partial x_j} + \frac{\partial u_j}{\partial x_i}\Big) \tag{1.28}$$

2. Elastic stress-strain law

$$\sigma_{ij} = C_{ijkl}\varepsilon_{kl} \tag{1.29}$$

3. Stress equilibrium equations

$$\frac{\partial \sigma_{ij}}{\partial x_i} + b_j = 0 \tag{1.30}$$

4. Boundary equations

$$u_i = u^* \text{ on } \partial_1 R \tag{1.31a}$$
$$\sigma_{ij} n_i = t_j^* \text{ on } \partial_2 R \tag{1.31b}$$

Now we have to get the displacement from weak form which is always obtained by replacing the stress equilibrium equation by an equivalent virtual work equation. So, as it is clear from weak form of equation, given in Appendix B, we have displacement field and velocity field, the interpolation of these filed is needed. The interpolated values for displacement field and velocity field are inserted into the weak form. Now the body is discretized in many finite elements and for each element one will use the interpolated form of equation to find displacement and then other values from other equations as mentioned. The values of displacement will be interpolated from element to element. Putting the displacement in $\varepsilon_{ij} = 1/2(\partial u_i/\partial x_j + \partial u_j/\partial x_i)$ and obtain the strain and then finally get the stresses from $\sigma_{ij} = C_{ijkl}\varepsilon_{kl}$ by inserting the values of strains.

1.8.2 Hyper-elasticity

The model discussed by *Simo and Miehe, 1992*[13] used the basics of hyperelastic models. It is based on the Neo-Hookean constitutive law.

Given Shape of the problem R, material constants μ_1 and $K_1$for Neo-Hookean law, mass density in its reference configuration ρ_0, body force distribution $\boldsymbol{b}$, initial stresses and thermal expansion coefficients (if given), boundary conditions (displacement on $\partial_1 R$ and traction boundary condition on $\partial_2 R$).

Calculate The displacement, deformation gradient, and Cauchy stresses (u_i, F_{ij},and σ_{ij}) while satisfying the governing equations and boundary conditions. Here we have:

$$y_i = x_i + u_i(x_k) \quad , \quad F_{ij} = \delta_{ij} + \frac{\partial u_i}{\partial x_j} \quad , \quad J = det(F) \quad \text{and} \quad \boldsymbol{b}_{ij} = F_{ik}F_{jk} \tag{1.32}$$

$$\frac{\partial \sigma_{ij}}{\partial x_i} + b_j = 0 \tag{1.33}$$

$$u_i = u^* \text{ on } \partial_1 R \tag{1.34a}$$
$$\sigma_{ij} n_i = t_j^* \text{ on } \partial_2 R \tag{1.34b}$$

with Cauchy stress related to the left Cauchy Green tensor by the Neo-Hookean constitutive law

$$\sigma_{ij} = \frac{\mu_1}{J^{5/3}}\Big(\boldsymbol{b}_{ij} - \frac{1}{3}\boldsymbol{b}_{kk}\delta_{ij}\Big) + K_1(J-1)\delta_{ij} \tag{1.35}$$

As always the stress equilibrium equation is replaced by the equivalent principle of virtual work which now has to be in a form appropriate for finite deformations. The virtual work equation can be given in terms of various types of stresses and deformation measures. Here the stresses are taken in terms of Kirchhoff stress as it is the most convenient.
The virtual work form of the equation is given in Appendix B. There are two additional terms in the stiffness matrix, which arises from the finite geometric deformations. The Kirchhoff stresses here depend on the displacement through deformation gradient. The strain measure can be taken as Hencky's logrithmic strain tensor. The Newton Raphson method is used to solve the virtual work equation. The tangent stiffness is solved after solving the left Cauchy Green tensor and finally the stresses are found through the neo-Hookean law.

1.8.3 Viscoplasticity

The viscoplasticity is about the history and time dependent materials modeling. As the *Simo and Miehe, 1992*[13] has explained the plasticity of finite strains, approximately a hyper-elastic model, but here a the small strain viscoplasticity is explained for an overview.

Given Shape of the problem R, material constants $Y, n, m, \dot{\varepsilon}_0, Q$ and ε_0(for viscoplastic creep law) , body force distribution $\boldsymbol{b}$, initial stresses and thermal expansion coefficients (if given), boundary conditions (displacement on $\partial_1 R$ and traction boundary condition on $\partial_2 R$).

Calculate the displacement, strain, and stress (u_i, ε_{ij},and σ_{ij}) while satisfying the following governing equations.

1. Strain-displacement equation

$$\varepsilon_{ij} = \frac{1}{2}\Big(\frac{\partial u_i}{\partial x_j} + \frac{\partial u_j}{\partial x_i}\Big) \tag{1.36}$$

2. Stress equilibrium equation

$$\frac{\partial \sigma_{ij}}{\partial x_i} + b_j = 0 \tag{1.37}$$

3. Boundary equations

$$u_i = u^* \text{ on } \partial_1 R \tag{1.38a}$$

$$\sigma_{ij} n_i = t_j^* \text{ on } \partial_2 R \tag{1.38b}$$

4. The constitutive equation for small strain, power law rate dependent plasticity is given below. It is important to note that this is one of the simplest case of plasticity. Plasticity with various internal variables and hardening parameters are not discussed here, but in chapeter three.

$$\dot{\varepsilon}_{ij} = \dot{\varepsilon}^e_{ij} + \dot{\varepsilon}^p_{ij} \tag{1.39}$$

Where,

$$\dot{\varepsilon}^e_{ij} = \frac{1+\nu}{E}\big(\dot{\sigma}_{ij} - \frac{\nu}{1+\nu}\dot{\sigma}_{kk}\delta_{ij}\big) \tag{1.40}$$

$$\dot{\varepsilon}^p_{ij} = \dot{\varepsilon}_0\, exp(-Q/kT)\Big(\frac{\sigma_e}{\sigma_0}\Big)^m \frac{3}{2}\frac{S_{ij}}{\sigma_e} \tag{1.41}$$

Where, E is the Young Modulus, and ν is the Poisson ration.

$$\sigma_0 = Y\Big(1 + \frac{\varepsilon_e}{\varepsilon_0}\Big)^{1/n} \tag{1.42a}$$

$$\sigma_e = \sqrt{\frac{2}{3}S_{ij}S_{ij}} \tag{1.42b}$$

$$S_{ij} = \sigma_{ij} - \frac{1}{3}\sigma_{kk}\delta_{ij} \tag{1.42c}$$

$$\dot{\varepsilon}_e = \sqrt{\frac{3}{2}\dot{\varepsilon}^p_{ij}\dot{\varepsilon}^p_{ij}} \tag{1.42d}$$

Where E, ν are the Elastic modulus and poisson ratio respectively (1.42e)

Now this is history dependent problem and one has to specify the time variation of the applied load and boundary conditions. Here we have to find the displacement, strain and then stresses as a function of time. Here the stress equilibrium equation is replaced by equivalent principle virtual work equation, and the displacements are found as function of time, and then the strains from the equation given above and then finally the stresses from the constitutive equation as a function of time.

Chapter 2

Thermo-Mechanical Coupled Problems in Solid Mechanics

In the current chapter, the plasticity models covered by Abaqus will be discussed as a first part. Secondly the general theory of thermoplasticity is explained briefly starting from the pure mechanics models of rate-independent plasticity. The inelasticity model narrated by Abaqus is necessary to know before modeling any type of material. They give an overall overview of all the models which are currently under observations all over the world. All the constitutive models in mechanics in all the universities are somehow related to the inelastic models discussed by Abaqus. So it is extremely important to know commercialized form of models before starting the modeling. Similarly the general frame work for thermoplasticity need to be well defined for each model before starting the numerical implementation.

2.1 Plasticity

The material library of the Abaqus includes the following models. These models are explained with the basics before starting the simulation in Abaqus. The main foundations of each model are detailed with reference to selection of the elements, theoretical frame work, time increment, numerical method, and references to the renowned papers and books.
For further detail, one can see the *User Manuals, section 19.1.1 (volume 3, Abaqus 6.8).*

- Classical metal plasticity
- Metal plasticity in cyclic loading
- Rate-dependent yield
- Creep and swelling
- Annealing or melting
- Anisotropic yield and creep

- Johnson-Cook plasticity
- Dynamic failure models
- Porous metal plasticity
- Cast iron plasticity
- Two-layer viscoplasticity
- ORNL constitutive model
- Deformation plasticity
- Extended Drucker-Prager plasticity and creep
- Modified Drucker-Prager/Cap plasticity and creep
- Mohr-Coulomb plasticity
- Critical state (clay) plasticity
- Crushable foam plasticity
- Jointed material
- Concrete
- Progressive damage and failure

Here in the current thesis, the classical metal plasticity model is used. This is mostly used to model the perfect plasticity, and plasticity with isotropic hardening at relatively low temperatures and small strains. It use the Mises or Hill yield surface with associated plastic flow. Each model can be further enriched by including other factors, e.g. rate dependency of strain, creep and swelling, anisotropy, kinematic hardening etc. The ORNL model (Oak-Ridge National Laboratory) is basically used to consider the factor of cyclic loading and high-temperature creep in 304 and 316 stainless steel grades which are mostly used in high temperature and high pressure applications, e.g. fertilizer industry, steam and gas power plants, fire-tube boilers, syn gas production zone etc. The models in the Abaqus include almost all sort of models; models for foam, concrete, porosity, fully plastic, polymers, clay, geological, sand, and many others. It is very important to know each point of modeling before the start of practical industrial material modeling, and here in this section of the Abaqus manuals, all the points are explained well.

2.2 Thermoplasticity

In early nineteenth century, the studies on mechanics of material lead to the development of plastic flow yielding criteria for metals and soils. Due to the lack of highly sophisticated measuring tools, the plasticity studies did not advanced much with time.

By the mid-twentieth century, the research carried to the rate-independent incompressible plastic flow in isotropic materials. The research explained the yield criteria and the relation between stress and rate of strain. The most successful yield criteria was of Von Mises.

Later on the the hardening effects were included by Taylor, Quinney, Schmidt, and Odquist and the constant yield criteria was replaced by a function of some hardening parameter. The hardening parameters were chosen to provide a suitable measure of the strain history and were usually represented by quantities like plastic work and plastic distortion.

At the same time, Saint-Venant, Levy, Prandtl, and Reusse proposed plastic flow rules which expressed the proportionality of deviatoric stress and deviatoric rate of plastic strain. For finding the complete solution at that time, the plastic flow rule combined with the yield criteria, the equilibrium condition for stress, and the boundary conditions, were sufficient to solve a boundary value problem of macroscopic plastic flow.

A rate-dependent generalization was provided by Sokolovsky and Malvern, and advanced by Perzyna. The rate-dependent theory was motivated by the observation of higher yield values for high loading rates, and was found to be more suitable in the dynamic studies of plasticity. The flow rules in rate-dependent theories are different than that of rate-independent theories, because one has to put effort in considering some suitable scales of time.

After some decades, the two major advancement were established regarding the geometric and thermodynamic nature of the plastic flow. These advances, e.g. by Kroner, Noll, and Edelen, proved the dislocations to be the main objects causing the plastic flow and they are distributed over the whole body.

At the same time, the plasticity was tried to be formulated under the frame work of thermodynamics. From the papers of Eckart and Bridgman, it became increasingly evident that a general theory of plasticity must has to satisfy the fundamental laws of thermodynamics. So, Kestin, Green and Naghdi introduced the plastic strain as the internal variable whose evolution contributes to the dissipation. Similarly postulates of maximum dissipation were provided by Drucker and Ilyushin, which established plastic flow rules for rateindependent materials and also provided restrictions on the nature of the yield surface. The postulate of maximum plastic dissipation is a stronger inequality than the second law of thermodynamics, which in itself is insufficient to establish a plastic flow rule.

In the last two decade and till now, there were more sophisticated advances including the computational filed of studies. Now the dislocations are studied with much variations in sizes, densities, strain-rates and many other internal variables. There is no need to tackle now millions of dislocations analytically. The concepts of condensed matter physics, nonlinear thermodynamics, and continuum mechanics are combined to formulate a well-founded theory of plasticity with an aim to understand both the micro-scale and the macro-scale

behavior of solids, with deformation processes occurring for a wide range of time durations, e.g. from instantaneous pattern formation to creep.
(The above hierarchical detail of plasticity was taken from Anurag Gupta's lecture notes on Theory of Plasticity, http://home.iitk.ac.in/ag/ME721/intro.pdf)

Here in the next section, the plasticity governing equations for 1-D, with isotropic hardening, kinematic hardening, and combined isotropic and kinematic hardening are given in the boxes. The models are taken from *Incremental Theory of Plasticity, by Dr. Sebastian Nervi, and Dr. Ricardo L. Actis, October 1, 2008*,[34]. In the end the positions of thermodynamics relations with mechanics are detailed.

2.2.1 An elementary model for isotropic hardening

There are two assumptions taken; First the hardening is isotropic, i.e. the center of the yield surface, E_σ, remains at origin at any loading condition. Second, the hardening is linear for the amount of plastic flow $\dot{\varepsilon}^p$ and independent of sign. These two assumptions are illustrated with the following figures.

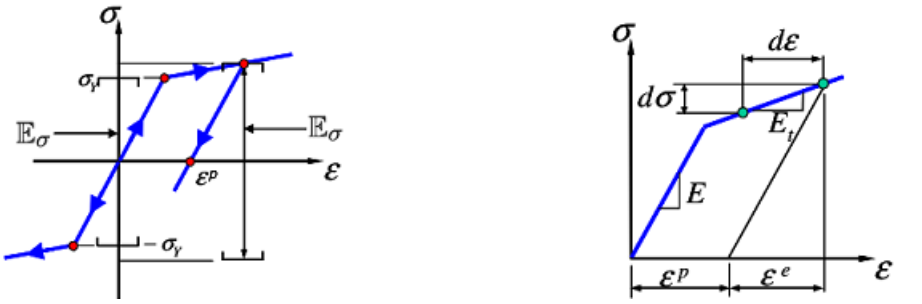

(a) Illustration of the center

(b) Illustration of the linearity

Figure 2.1: Assumptions used for isotropic hardening

Th admissible stresses can be defined as

$$\boxed{\boldsymbol{E}_\sigma = \{(\boldsymbol{\sigma}, \boldsymbol{\alpha}) \in \boldsymbol{R} \times \boldsymbol{R} \quad | \quad \boldsymbol{f}(\boldsymbol{\sigma}, \boldsymbol{\alpha}) = |\boldsymbol{\sigma}| - [\boldsymbol{\sigma}_y + \boldsymbol{K}\boldsymbol{\alpha}] \leq 0\}}$$

The constitutive model is summarized in Box 1.

i- Elastic strain relationship

$$\boldsymbol{\sigma} = \boldsymbol{E}(\boldsymbol{\varepsilon} - \boldsymbol{\varepsilon}^p)$$

ii- Flow rule and isotropic hardening law

$$\dot{\boldsymbol{\varepsilon}}^p = \boldsymbol{\gamma}\frac{\boldsymbol{\partial f}}{\boldsymbol{\partial \sigma}} = \boldsymbol{\gamma} sign(\boldsymbol{\sigma})$$

$$\dot{\boldsymbol{\alpha}} = \boldsymbol{\gamma}$$

iii- Yield condition

$$\boldsymbol{f}(\boldsymbol{\sigma}, \boldsymbol{\alpha}) = |\boldsymbol{\sigma}| - \left(\boldsymbol{\sigma}_y + \boldsymbol{K\alpha}\right) \leq \mathbf{0}$$

iv- Kuhn-Tucker complementary conditions

$$\boldsymbol{\gamma} \geq \mathbf{0}, \quad \boldsymbol{f}(\boldsymbol{\sigma}, \boldsymbol{\alpha}) \leq \mathbf{0}, \quad \boldsymbol{\gamma f}(\boldsymbol{\sigma}, \boldsymbol{\alpha}) = \mathbf{0}$$

v- Consistency conditions

$$\dot{\boldsymbol{\gamma}}\dot{\boldsymbol{f}}(\boldsymbol{\sigma}, \boldsymbol{\alpha}) = \mathbf{0} \text{ (if } \boldsymbol{f}(\boldsymbol{\sigma}, \boldsymbol{\alpha}) = \mathbf{0})$$

Box 1: Constitutive model of thermoplasticity with isotropic Hardening

2.2.2 An elementary model for kinematic hardening

There are also two assumptions, the hardening is kinematic as the size of the yield surface $\boldsymbol{E}_\sigma$ cannot change and its center can move with respect to the origin at any loading. The second assumption is also almost the same, as the hardening is linear for the amount of plastic flow $\dot{\varepsilon}^p$ and independent of sign. These two assumptions are illustrated with the following figures.

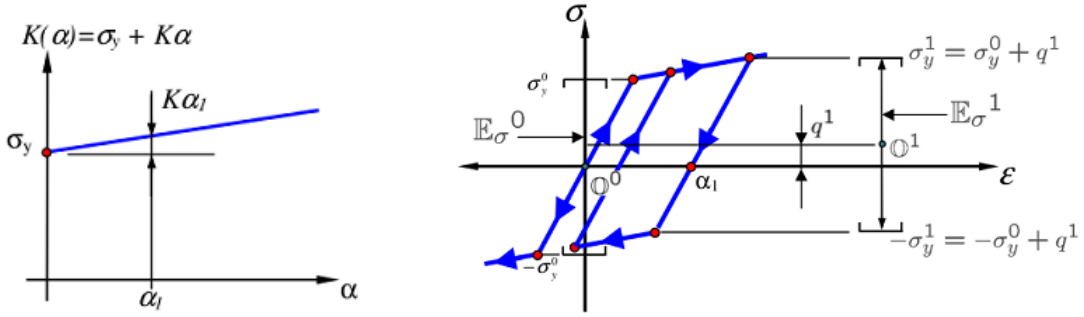

(a) Illustration of the center

(b) Illustration of the linearity

Figure 2.2: Assumptions used for kinematic hardening

The admissible stress range can be written as:

$$\boldsymbol{E}_\sigma = \{(\boldsymbol{\sigma}, \boldsymbol{\alpha}) \in \boldsymbol{R} \times \boldsymbol{R} \quad | \quad \boldsymbol{f}(\boldsymbol{\sigma}, \boldsymbol{\alpha}) = |\boldsymbol{\sigma} - \boldsymbol{q}| - \boldsymbol{\sigma}_y \leq 0\}$$

The constitutive model is summarized in Box 2.

i- Elastic strain relationship

$$\boldsymbol{\sigma} = \boldsymbol{E}(\boldsymbol{\varepsilon} - \boldsymbol{\varepsilon}^p)$$

ii- Flow rule and isotropic hardening law

$$\dot{\boldsymbol{\varepsilon}}^p = \boldsymbol{\gamma}\frac{\boldsymbol{\partial f}}{\boldsymbol{\partial \sigma}} = \boldsymbol{\gamma} sign(\boldsymbol{\sigma})$$

$$\dot{\boldsymbol{\alpha}} = \boldsymbol{\gamma}$$

iii- Yield condition

$$\boldsymbol{f}(\boldsymbol{\sigma}, \boldsymbol{\alpha}) = |\boldsymbol{\sigma} - \boldsymbol{q}| - \boldsymbol{\sigma}_y \leq \boldsymbol{0}$$

$$\boldsymbol{q} = sign(\boldsymbol{\sigma} - \boldsymbol{q})\boldsymbol{K}\boldsymbol{\alpha}$$

iv- Khun-Tucker complementary conditions

$$\boldsymbol{\gamma} \geq \boldsymbol{0}, \quad \boldsymbol{f}(\boldsymbol{\sigma}, \boldsymbol{\alpha}) \leq \boldsymbol{0}, \quad \boldsymbol{\gamma f}(\boldsymbol{\sigma}, \boldsymbol{\alpha}) = \boldsymbol{0}$$

v- Consistency conditions

$$\dot{\boldsymbol{\gamma}}\dot{\boldsymbol{f}}(\boldsymbol{\sigma}, \boldsymbol{\alpha}) = \boldsymbol{0} \text{ (if } \boldsymbol{f}(\boldsymbol{\sigma}, \boldsymbol{\alpha}) = \boldsymbol{0})$$

Box 2: Constitutive model of thermoplasticity with kinematic Hardening

2.2.3 An elementary model for mixed hardening

Here, it is assumed that the hardening is both isotropic and kinematic, i.e. the size of the yield surface, $\boldsymbol{E}_\sigma$ can be increased, and the center of the yield surface can be moved with respect to origin. The assumption is explained through the the following diagram. The set

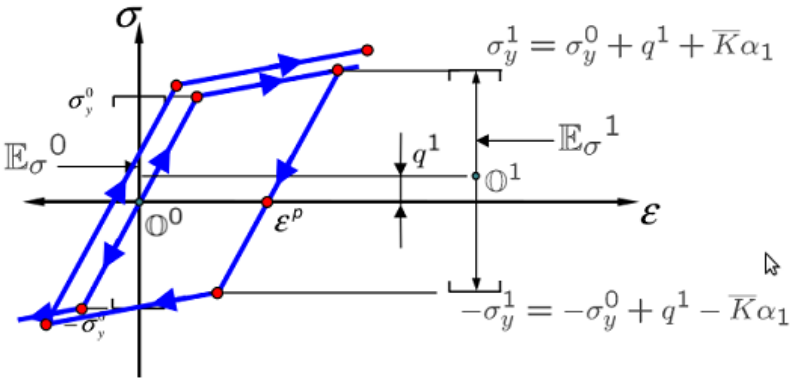

Figure 2.3: Illustration of mixed hardening

of admissible stresses can be defined as;

$$\boldsymbol{E}_\sigma = \{(\boldsymbol{\sigma}, \boldsymbol{\alpha}) \in \boldsymbol{R} \times \boldsymbol{R} \quad | \quad \boldsymbol{f}(\boldsymbol{\sigma}, \boldsymbol{\alpha}) = |\boldsymbol{\sigma} - \boldsymbol{q}| - [\boldsymbol{\sigma}_y + \bar{\boldsymbol{K}}\boldsymbol{\alpha}] \leq 0\}$$

i- Elastic strain relationship

$$\boldsymbol{\sigma} = \boldsymbol{E}(\boldsymbol{\varepsilon} - \boldsymbol{\varepsilon}^p)$$

ii- Flow rule and isotropic hardening law

$$\dot{\boldsymbol{\varepsilon}}^p = \boldsymbol{\gamma}\frac{\boldsymbol{\partial f}}{\boldsymbol{\partial \sigma}} = \boldsymbol{\gamma} sign(\boldsymbol{\sigma})$$

$$\dot{\boldsymbol{\alpha}} = \boldsymbol{\gamma}$$

iii- Yield condition

$$\boldsymbol{f}(\boldsymbol{\sigma}, \boldsymbol{\alpha}) = |\boldsymbol{\sigma} - \boldsymbol{q}| - \left(\boldsymbol{\sigma}_y + \bar{\boldsymbol{K}}\boldsymbol{\alpha}\right) \leq \boldsymbol{0}$$

$$\boldsymbol{q} = sign(\boldsymbol{\sigma} - \boldsymbol{q})\boldsymbol{\beta K \alpha}$$

$$\bar{\boldsymbol{K}} = (1 - \boldsymbol{\beta})\boldsymbol{K}$$

iv- Khun-Tucker complementary conditions

$$\boldsymbol{\gamma} \geq \boldsymbol{0}, \quad \boldsymbol{f}(\boldsymbol{\sigma}, \boldsymbol{\alpha}) \leq \boldsymbol{0}, \quad \boldsymbol{\gamma f}(\boldsymbol{\sigma}, \boldsymbol{\alpha}) = \boldsymbol{0}$$

v- Consistency conditions

$$\dot{\boldsymbol{\gamma}}\dot{\boldsymbol{f}}(\boldsymbol{\sigma}, \boldsymbol{\alpha}) = \boldsymbol{0} \text{ (if } \boldsymbol{f}(\boldsymbol{\sigma}, \boldsymbol{\alpha}) = \boldsymbol{0})$$

Box 3: Constitutive model of thermoplasticity with mixed Hardening

2.2.4 Thermoplasticity with isotropic hardening

As the thermodynamics frame work was developed to study the mechanics under thermal effects, so there was a need to define some state variables,and these state variables were named as internal variables. These variables were introduced in order to verify or justify the increase of yield strenght due to strain effects at micro and macro level. Similarly there was a need to justify the temperature increase in the body under plastic strain, so the second law of thermodynamics need to be consider if there are some temperature changes. A term of free energy was introduced in order to justify heat dissipation due to mechanical power.

In order to find the number of internal variables for introducing in the body, it is necessary to find the the number of ways in which one can store the energy in the body. These ways can be strain (elastic or plastic), latent heat, temperature etc. There are some variables introduced for isotropic hardening and also for kinematic hardening. A variable entropy was explained in order to cope with temperature changes, and principle of maximum dissipation were introduced for heat dissipation, either latent or entered from surrounding. Similarly, some other variables can be introduced in order to justify or include the influence of the other theories, e.g. the isomorphism effects, as *A. Bertram* in his paper, *Finite thermoplasticity based on isomorphisms: April, 2003 (Otto-von-Guericke-Universita 39106 Magdeburg, Germany)*, [35], introduced ε_c and η_c, the new terms to justify the isomorphism. So, the thing is to match the theoretical and computational studies with the experimental and real graphs and values by introducing the new variables, either in tensor form, vector or scalar

form.
Here in the following box 4, isotropic model of thermoplasticity is detailed. The model is taken from *Simo and Miehe, 1992.*,[13].

i- Free energy function $[\hat{T}''' = \partial^2_{\theta\theta}\hat{\boldsymbol{M}}(\boldsymbol{J},\boldsymbol{\theta}) = 0\,]$:

$$\hat{\boldsymbol{\psi}} = \underbrace{\hat{\boldsymbol{T}}(\boldsymbol{\theta}) + \hat{\boldsymbol{M}}(\boldsymbol{J},\boldsymbol{\theta})}_{thermal} + \underbrace{\hat{\boldsymbol{U}}(\boldsymbol{J}) + \hat{\boldsymbol{W}}(\bar{\boldsymbol{b}}^e)}_{hyperelastic} + \underbrace{\hat{\boldsymbol{K}}(\boldsymbol{\alpha})}_{hardening}$$

ii- Kirchoff stress and entropy $[\boldsymbol{b^e} = \boldsymbol{F^e F^{et}} = \boldsymbol{F G^p F^t};\ \bar{\boldsymbol{b}}^e = J^{-2/3}\boldsymbol{b}^e\,]$:

$$\boxed{\boldsymbol{\tau} = pJ1 + dev\,[\boldsymbol{\tau}\,]} \qquad \boxed{\eta = \eta^t + \eta^e + \eta^p}$$

$$p = \hat{U}'(J) + \partial_j \hat{M}(\theta, J), \qquad \eta^t = -\hat{T}'(\theta)$$
$$dev\,[\boldsymbol{\tau}\,] = 2dev\,[\bar{\boldsymbol{b}}^e \partial_{\bar{b}^e}\hat{\boldsymbol{W}}(\bar{\boldsymbol{b}}^e)\,], \qquad \eta^e = -\partial_\theta \hat{\boldsymbol{M}}(\boldsymbol{J},\boldsymbol{\theta}),$$

iii- Von Mises yield criterion:

$$\hat{\boldsymbol{\phi}} = \|\mathrm{dev}\,[\boldsymbol{\tau}\,]\| - \sqrt{\frac{2}{3}}\,[\hat{K}'(\alpha) + \hat{\mathrm{y}}(\boldsymbol{\theta})\,] \le 0$$

iv- Evolution equations $[\lambda \ge 0, \lambda\hat{\boldsymbol{\phi}} = 0, \partial_\tau\hat{\boldsymbol{\phi}} = dev\,[\boldsymbol{\tau}\,]/\|dev\,[\boldsymbol{\tau}\,]\|\,]$:

$$\boldsymbol{\mathcal{L}}_v \boldsymbol{b}^e = -2\lambda\,[\partial_\tau\hat{\boldsymbol{\phi}}\,]\boldsymbol{b}^e,$$

$$\dot{\eta}^p = -\sqrt{\frac{2}{3}}\lambda\boldsymbol{\theta}\hat{y}'(\boldsymbol{\theta})$$
$$\dot{\alpha} = \sqrt{\frac{2}{3}}\lambda$$

v- Capacity, mechanical dissipation, elastic heating, heat flux:

$$c = -\theta\hat{T}''(\theta)$$

$$\mathcal{D}_{mech} = \hat{y}(\boldsymbol{\theta})\sqrt{\frac{2}{3}}\lambda$$
$$\mathcal{H} = -\theta\partial^2_{\theta\theta}\hat{\boldsymbol{M}}(\boldsymbol{J},\boldsymbol{\theta})\dot{J},$$
$$\boldsymbol{q} = -\,[k1\,]\nabla\theta$$

Box 4: Simo and Miehe Isotropic model of thermoviscoplasticity, (1992)[13]

Chapter 3

Review of Reference Papers in Thermo-visco-Plasticity

3.1 J.C. Simo and C. Miehe; Jan,1991 [13]:

Introduction:

The paper, *J.C. Simo, C. Miehe, Associative coupled thermo-plasticity*, is considered as a bench mark paper in the studies of thermoplasticity both with reference to governing equations and numerical formulation. Many of the authors later mentioned the reference from this paper. The governing equations and computational implementation are explained thoroughly for isothermal, non-isothermal, non-isothermal adiabatic, and non-isothermal convective problems are discussed in the paper with the help of renowned representative examples which later on were discussed by many of the authors as a reference solution.

Local governing equations for thermoplasticity:

The local governing equations in *Simo and Miehe* starts from thermoelastic domain, describing the internal energy, entropy, kinematic relations, free energy, local dissipation, constitutive equations, evolution equations,maximum dissipation, interpretation of the flow rule, temperature evolution equation and ended by summarizing the model of J_2 flow theory.
The elastic domain expressed in terms of the true stresses and in current configuration is given by;

$$\mathbb{E} = \{(\boldsymbol{\tau}, \boldsymbol{\beta}, \boldsymbol{\theta}) : \hat{\boldsymbol{\phi}}(\boldsymbol{\tau}, \boldsymbol{\beta}, \boldsymbol{\theta}) \leq 0\} \tag{3.1}$$

Where $\boldsymbol{\tau}$ is the Kirchoff stress tensor, $\boldsymbol{\beta}$ is the vector of internal variables and $\boldsymbol{\theta}$ is the absolute temperature. The classical Von Mises yield criterion is expressed by;

$$\hat{\boldsymbol{\phi}}(\boldsymbol{\tau}, \boldsymbol{\beta}, \boldsymbol{\theta}) = \|\mathrm{dev}\,[\boldsymbol{\tau}\,]\| + \sqrt{\frac{2}{3}}\,[\boldsymbol{\beta} - \hat{\mathrm{y}}(\boldsymbol{\theta})\,] \leq 0 \tag{3.2}$$

3.1.1 Internal energy and plastic configurational entropy

Simo and Miehe described the internal energy as;

$$e = \hat{e}(\boldsymbol{X}; \boldsymbol{C}, \boldsymbol{\Gamma}, \eta - \eta^p) \tag{3.3}$$

Where, $\boldsymbol{X}$ is related to the possible in-homogeneities in the lattice structure, $\boldsymbol{C}$ is the left Cauchy Green deformation tensor, $\boldsymbol{\Gamma}$ is the set of strain-line internal variables responsible for inelastic response of the material,η is the total entropy of the material and η^p is the plastic entropy of the material which is also introduced as an internal variable.
Many of the model were introduced by neglecting the thermal part in plasticity(i.e there is no $\eta - \eta^p$ term).

3.1.2 Kinematic relations for multiplicative decomposition

According to Taylor et al. [6],Simo and Miehe considered the local multiplicative decomposition of deformation gradient, $\boldsymbol{F} = \boldsymbol{F^e F^p}$ and introduced the two strain measures associated with reference and current configurations.

$$\boldsymbol{G^p} = [\boldsymbol{F^{pt} F^p}]^{-1} \quad \text{and} \quad \boldsymbol{b^e} = \boldsymbol{F^e F^{et}} \tag{3.4}$$

The two relations are related by;

$$\boldsymbol{b^e} = \boldsymbol{F G^p F^t} \quad \text{and} \quad \boldsymbol{1} = \boldsymbol{F^{-t} C F^{-1}} \tag{3.5}$$

The time differentiation of the above equation give the following relations.

$$\boldsymbol{b^e} = \boldsymbol{l b^e} + \boldsymbol{b^e l^t} + \boldsymbol{\mathcal{L}_v b^e} \quad \text{with} \quad \boldsymbol{\mathcal{L}_v b^e} = \boldsymbol{F \dot{G}^p F^t} \tag{3.6}$$

where $\boldsymbol{l}$ is the velocity gradient and $\boldsymbol{\mathcal{L}_v b^e}$ is called the Lie derivative of elastic left Cauchy Green tensor $\boldsymbol{b^e}$.

3.1.3 Free energy, local dissipation and constitutive equations

The free energy takes the following form:

$$e = \hat{e}(\boldsymbol{b^e}, \alpha, \eta^e), \quad \text{with} \quad \eta^e = \eta - \eta^p \tag{3.7}$$

Where η^p is the plastic entropy.
By Legendre transformation, we get the free energy function $\hat{\psi}$ by subtracting the entropy of the material from the internal energy of the material.

$$\hat{\psi}(\boldsymbol{b^e}, \alpha, \boldsymbol{\theta}) = \hat{e}(\boldsymbol{b^e}, \alpha, \eta^e) - \eta^e \boldsymbol{\theta} \tag{3.8}$$

Reduced dissipation inequality:

According to Clausius Plank form of second law of thermodynamics(which is only the local dissipation inequality).

$$\mathcal{D} = \boldsymbol{\theta}\gamma_{loc} = \boldsymbol{\theta}\dot{\eta} + \boldsymbol{\tau}\cdot\boldsymbol{d} - \dot{e} \geq 0 \tag{3.9}$$

Where $\boldsymbol{d}$ is the symmetric part of velocity gradient. Inserting the values of $\dot{e}$ and $\dot{\eta}$ into the Clausius Plank form of second law of thermodynamics, we get the dissipation inequality. But it should be noted that $\eta = \eta^e + \eta^p$; and $\hat{\psi}$ depends on three variables, $\boldsymbol{b^e}$, α, and $\boldsymbol{\theta}$.

$$\mathcal{D} = [-(\eta-\eta^p)-\partial_\theta\hat{\psi}]\dot{\boldsymbol{\theta}} + [\boldsymbol{\tau}-2\partial_{b^e}\hat{\psi}\boldsymbol{b}^e]\cdot\boldsymbol{d} + [2\partial_{b^e}\hat{\psi}\boldsymbol{b}^e]\cdot[-\frac{1}{2}(\boldsymbol{\mathcal{L}}_v\boldsymbol{b}^e)\boldsymbol{b}^{e-1}] + [-\partial_\alpha\hat{\psi}]\dot{\alpha} + \boldsymbol{\theta}\dot{\eta}^p \geq 0 \tag{3.10}$$

It gives the following constitutive equations (see e.g. [51, 49]).

$$\boldsymbol{\tau} = 2\partial_{b^e}\hat{\psi}\boldsymbol{b}^e \quad \text{and} \quad \eta = \eta^p - \partial_\theta\hat{\psi} \tag{3.11}$$

By setting $\boldsymbol{\beta} = -\partial_\alpha\hat{\psi}$, the reduced form of the dissipation inequality can be written as;

$$\mathcal{D} = \underbrace{\boldsymbol{\tau}\cdot[-\frac{1}{2}(\boldsymbol{\mathcal{L}}_v\boldsymbol{b}^e)\boldsymbol{b}^{e-1}] + \boldsymbol{\beta}\dot{\alpha}}_{\mathcal{D}_{mech}} + \underbrace{\boldsymbol{\theta}\dot{\eta}^p}_{\mathcal{D}_{ther}} \geq 0 \tag{3.12}$$

The term $\mathcal{D}_{ther}$ is the new term by *Simo and Miehe*, and shows the pure thermal dissipation in the form of entropy production, $\dot{\eta}^p$ introduced earlier in the internal energy as an internal variable.

3.1.4 Evolution equations; maximum dissipation

Now the evolution equations for all internal variables are derived according to the Principle of maximum plastic work defined by Von Mises (see [6]) which says that the total dissipation is always maximum in the material. Here *Simo and Miehe* extended this principle of maximum dissipation to thermomechanical problems and resulted that the maximum dissipation depends on the plastic entropy which they have introduced.

Thermomechanical principle of maximum dissipation:

The maximum dissipation principle for thermomechanical problems can be written as;

$$[\boldsymbol{\tau} - \overset{*}{\boldsymbol{\tau}}]\cdot[-\frac{1}{2}(\boldsymbol{\mathcal{L}}_v\boldsymbol{b}^e)\boldsymbol{b}^{e-1}] + [\boldsymbol{\beta} - \overset{*}{\boldsymbol{\beta}}]\dot{\alpha} + [\boldsymbol{\theta} - \overset{*}{\boldsymbol{\theta}}]\dot{\eta}^p \geq 0 \tag{3.13}$$

It is assumed to hold for all admissible $\overset{*}{\boldsymbol{\tau}}$, $\overset{*}{\boldsymbol{\beta}}$ and $\overset{*}{\boldsymbol{\theta}}$. If the elastic domain is given by the first equation as mentioned in the start, then the evolution equations can be obtained as;

$$-\frac{1}{2}\boldsymbol{\mathcal{L}}_v\boldsymbol{b}^e = \lambda[\partial_\tau\hat{\boldsymbol{\phi}}]\boldsymbol{b}^e, \qquad \dot{\alpha} = \lambda\partial_\beta\hat{\boldsymbol{\phi}}\ , \qquad \dot{\eta}^p = \lambda\partial_\theta\hat{\boldsymbol{\phi}}\ , \tag{3.14}$$

Where λ is the Lagrange multiplier and satisfy the Kuhn-Tucker conditions,

$$\lambda \geq 0\ , \qquad \hat{\boldsymbol{\phi}}(\boldsymbol{\tau},\boldsymbol{\beta},\boldsymbol{\theta}) \leq 0\ , \qquad \lambda\hat{\boldsymbol{\phi}}(\boldsymbol{\tau},\boldsymbol{\beta},\boldsymbol{\theta}) = 0 \tag{3.15}$$

Interpretation of the flow rule:

The flow rule $-\frac{1}{2}\boldsymbol{\mathcal{L}}_v \boldsymbol{b}^e = \lambda\,[\partial_\tau \hat{\boldsymbol{\phi}}\,]\boldsymbol{b}^e$, in the above equation is interpreted with reference to pressure insensitivity of yield criterion and showed that $\boldsymbol{tr}\,[\partial_\tau \hat{\boldsymbol{\phi}}\,] = 0$ and $\boldsymbol{J}^p = 1$.
The flow rule is also expressed in terms of intermediate configuration for Piola-Kirchoff stresses as below.

$$sym\,[\boldsymbol{L}^p\,] = \lambda \boldsymbol{N}\boldsymbol{C}^e\ , \qquad \text{where } \boldsymbol{C}^e = \boldsymbol{F}^{et}\boldsymbol{F}^e\ , \text{ and } \boldsymbol{L}^p = \dot{\boldsymbol{F}}^p\boldsymbol{F}^{p-1} \tag{3.16}$$

The flow rule is also tried to extend for rate-temperature dependent response of the material, where the Kuhn-Tucker conditions are replaced by constitutive equations.

3.1.5 The temperature evolution equation

Here the local balance of energy equation reduces to,

$$-\,\boldsymbol{J}div\,[\boldsymbol{q}/\boldsymbol{J}\,] + \mathcal{R} = \dot{e} - \boldsymbol{\tau}\cdot\boldsymbol{d} \tag{3.17}$$

Inserting the value of $\dot{e} - \boldsymbol{\tau}\cdot\boldsymbol{d}$ from Clausius Plank form of second law of thermodynamics in equation (3.17), we get

$$-\,\boldsymbol{J}div\,[\boldsymbol{q}/\boldsymbol{J}\,] + \mathcal{R} = \boldsymbol{\theta}\dot{\eta} - \mathcal{D} = \boldsymbol{\theta}(\dot{\eta} - \dot{\eta}^p) - \mathcal{D}_{mech} \tag{3.18}$$

From the reduced dissipation inequality and the corresponding constitutive equations we get the evolution equation for total entropy as

$$\boldsymbol{\theta}\dot{\eta} = \boldsymbol{\theta}\dot{\eta}^p - \boldsymbol{\theta}\partial_\theta\dot{\hat{\psi}} = \boldsymbol{\theta}\dot{\eta}^p + c\dot{\boldsymbol{\theta}} + \mathcal{H}, \tag{3.19}$$

Where $\mathcal{H}$ is the elastic-plastic structural heating. It is associated with the non-dissipative (latent) elastic and plastic structural changes. Here the structural heating is given as;

$$\mathcal{H} = -\boldsymbol{\theta}[\partial_{\theta b^e}\hat{\psi}\cdot\dot{b}^e + \partial_{\theta\alpha}\hat{\psi}\dot{\boldsymbol{\alpha}}] \tag{3.20}$$

Substituting the evolution equation of total entropy into the equation (3.18), we get the temperature evolution equation

$$c\dot{\boldsymbol{\theta}} = \,[\mathcal{D}_{mech} - \mathcal{H}\,] + \,[-\boldsymbol{J}div\,[\boldsymbol{q}/\boldsymbol{J}\,] + \mathcal{R}\,] \tag{3.21}$$

In adiabatic case, the second bracket vanishes. The constitutive equation for heat flux is defined by the Fourier's Law

$$\boldsymbol{q} = -k\nabla\boldsymbol{\theta} \tag{3.22}$$

3.1.6 Application: A thermomechanical model of J_2-flow theory

Considering the given elastic domain, flow rules and evolution equations for entropy and temperature, the J_2 flow theory can be modeled with the following specific form of free energy function;

$$\hat{\psi} = \underbrace{\hat{\boldsymbol{T}}(\boldsymbol{\theta}) + \hat{\boldsymbol{M}}(\boldsymbol{J},\boldsymbol{\theta})}_{thermal} + \underbrace{\hat{\boldsymbol{U}}(\boldsymbol{J}) + \hat{\boldsymbol{W}}(\bar{\boldsymbol{b}^e})}_{hyperelastic} + \underbrace{\hat{\boldsymbol{K}}(\boldsymbol{\alpha})}_{hardening} \tag{3.23}$$

Since total dissipation is given by $\mathcal{D} = \mathcal{D}_{mech} + \mathcal{D}_{ther}$, by substituting the evolution equations, and using the Von Mises yield criterion, we get the simplified forms of $\mathcal{D}_{mech}$ and $\mathcal{D}_{ther}$ as

$$\mathcal{D}_{mech} = \sqrt{\frac{2}{3}}\hat{y}(\boldsymbol{\theta})\lambda \qquad \text{and} \qquad \mathcal{D}_{ther} = -\sqrt{\frac{2}{3}}\lambda\boldsymbol{\theta}\,\hat{y}'(\boldsymbol{\theta}) \tag{3.24}$$

Considering the generalized form of linear isotropic elastic hardening,

$$\hat{\boldsymbol{U}}(\boldsymbol{J}) = \kappa\,[\frac{1}{2}(\boldsymbol{J}^2 - 1) - ln\,\boldsymbol{J}\,] \quad \text{and} \quad \hat{\boldsymbol{W}}(\bar{\boldsymbol{b}^e}) = \frac{1}{2}\mu\,[tr\,[\bar{\boldsymbol{b}^e}\,] - 3\,] \tag{3.25}$$

An explicit expressions for $\hat{\boldsymbol{T}}(\boldsymbol{\theta})$ and $\hat{\boldsymbol{M}}(\boldsymbol{J},\boldsymbol{\theta})$ is obtained as:

$$\hat{\boldsymbol{T}}(\boldsymbol{\theta}) = c\,[(\boldsymbol{\theta} - \boldsymbol{\theta}_0) - \boldsymbol{\theta}\,log\,[\boldsymbol{\theta}/\boldsymbol{\theta}_0\,]\,]\;, \quad \hat{\boldsymbol{M}}(\boldsymbol{J},\boldsymbol{\theta}) = (\boldsymbol{\theta} - \boldsymbol{\theta}_0)\hat{\boldsymbol{G}}(\boldsymbol{J}) \tag{3.26}$$

Where $\hat{\boldsymbol{G}}(\boldsymbol{J})$ is the function contributing for the thermal expansion, and is given by,

$$\hat{\boldsymbol{G}}(\boldsymbol{J}) = -3\boldsymbol{\beta}\hat{\boldsymbol{U}}'(\boldsymbol{J}) \tag{3.27}$$

3.2 Marko Canadijia, Josip Brnic; November, 2003 [29]:

Introduction:

The paper by *Marko Canadijia and Josip Brnic* deals with associative coupled thermo-plasticity at finite strains and based on the multiplicative decomposition of deformation gradient. The exception in this paper is the temperature dependence of all the material properties. A variational formulation is carried by mixed finite element method. There are some new terms in the tangent operators and structural elasto-plastic heating due to the temperature dependence of the material properties. This paper is also restricted to isotropic hardening and hyperelastic formulation as was of classical *Simo and Miehe* paper. This may cause some problem like anisotropic modeling, the problem discussed with the help of isomorphism by *Bertram, 2003*[35] and *Dachkovski and Böhm, 2004*. The basic equations under the classical headings are given here briefly.

3.2.1 Basic Kinematics

Here in the paper by *Marko Canadijia and Josip Brnic*, the two strain measures are taken, the plastic part of the right Cauchy -Green tensor

$$\boldsymbol{C}^p = (\boldsymbol{F}^p)^T \boldsymbol{F}^p \tag{3.28}$$

and the elastic left Cauchy-Green tensor

$$\boldsymbol{b}^e = \boldsymbol{F}(\boldsymbol{C}^p)^{-1} \boldsymbol{F}^T \tag{3.29}$$

3.2.2 Balance equations

The local form of momentum and energy balance equations are taken as

$$\left.\begin{array}{l} \rho_0 \dot{\boldsymbol{V}} = div\boldsymbol{P} + \bar{\boldsymbol{f}} \\ \rho_0 \dot{\boldsymbol{E}} + div\boldsymbol{Q} = \boldsymbol{S} \cdot \boldsymbol{D} + \rho_0 \dot{\boldsymbol{R}} \end{array}\right\} \text{ for } \Omega \text{ , and } t = [0,\, T] \tag{3.30}$$

The free energy is obtained by Legendre transformation, and the free energy function here is taken the same as Miehe.

$$e = \hat{e}(\boldsymbol{b^e}, \xi, \eta^e), \quad \text{and} \quad \psi = e - \boldsymbol{\theta}\eta \tag{3.31}$$

The ξ represents the internal strain hardening variable.
Thermomechanical model is completed by calculating the free energy function, constitutive equation for heat flux vector, evolution equation for internal variable, flow rules and evolution equation for temperature It should be noted that the Principle of objectivity restricts the above theory to isotropic materials, so dealing with anisotropic materials would cause problem.

3.2.3 Model of J_2-flow theory; multiplicative plasticity

The basis of stress tensor calculation in hyperelastic materials is the Helmholtz free energy function. The free energy function here is

$$\hat{\boldsymbol{\psi}} = \hat{\boldsymbol{T}}(\boldsymbol{\theta}) + \hat{\boldsymbol{M}}(\boldsymbol{J}, \boldsymbol{\theta}) + \hat{\boldsymbol{U}}(\boldsymbol{J}, \boldsymbol{\theta}) + \hat{\boldsymbol{W}}(\bar{\boldsymbol{b}}^e, \boldsymbol{\theta}) + \hat{\boldsymbol{K}}(\boldsymbol{\xi}, \boldsymbol{\theta}) \tag{3.32}$$

The difference in *Marko Canadijia and Josip Brnic* paper is that here is the additional term $\boldsymbol{\theta}$ in the last three terms. Also the heat capacity $c(\boldsymbol{\theta})$ in the purely thermal part, $\hat{\boldsymbol{T}}(\boldsymbol{\theta})$ which represents the purely thermal entropy, is different from *Simo and Miehe, 1992* paper.

$$c(\boldsymbol{\theta}) = -\boldsymbol{\theta}\partial^2_{\theta\theta}\hat{\boldsymbol{\psi}} = -\boldsymbol{\theta}\partial^2_{\theta\theta}\hat{\boldsymbol{T}} - \boldsymbol{\theta}\partial^2_{\theta\theta}(\hat{\boldsymbol{M}} + \hat{\boldsymbol{U}} + \hat{\boldsymbol{W}} + \hat{\boldsymbol{K}}) \tag{3.33}$$

$$c(\boldsymbol{\theta}) = c_0(\boldsymbol{\theta}) - \boldsymbol{\theta}\partial^2_{\theta\theta}(\hat{\boldsymbol{M}} + \hat{\boldsymbol{U}} + \hat{\boldsymbol{W}} + \hat{\boldsymbol{K}}) \tag{3.34}$$

Similarly, the values for $\hat{\boldsymbol{M}}$, $\hat{\boldsymbol{U}}$, $\hat{\boldsymbol{W}}$, $\hat{\boldsymbol{K}}$ and $\boldsymbol{H}(\xi)$ are explained onward. But this paper from *Marko Canadijia and Josip Brnic*, also deals the case of linear isotropic hardening, and this is clear by looking at the functions of $\hat{\boldsymbol{K}}$, $\boldsymbol{H}(\xi)$ and linear softening functions $y_0(\theta)$, $h(\theta)$ and $y_\infty(\theta)$.

3.2.4 Local dissipation inequalities

The momentum and energy balance equations for a body is constrained by second law of thermodynamics, in other words they have to be within the second law of thermodynamics. In the current paper, the law is mentioned in the form narrated by *Truesdell and Noll, 1965*[36].

$$\left.\begin{aligned}\gamma_{loc} &= \dot{\eta} - \tfrac{r}{\theta} + \tfrac{1}{\rho\theta} div\boldsymbol{q} \geq 0 \\ \gamma_{con} &= -\tfrac{\boldsymbol{q}}{\theta^2}\cdot\nabla\theta \geq 0\end{aligned}\right\} \tag{3.35}$$

Considering the local energy balance of material and the Legendre transformation, one get the following dissipation inequality.

$$\mathcal{D} = \boldsymbol{\theta}\gamma_{loc} + \boldsymbol{\theta}\gamma_{cond} = \overbrace{\underbrace{\boldsymbol{\theta}\dot{\eta} + \boldsymbol{\tau}\cdot\boldsymbol{d} - \dot{e}}_{\mathcal{D}_{mech}+\mathcal{D}_{ther}} - \underbrace{\frac{1}{\theta}\boldsymbol{q}\cdot\nabla\theta}_{\mathcal{D}_{cond}\geq 0}}^{internal\ dissipation} \geq 0 \tag{3.36}$$
$$\mathcal{D}_{loc}\geq 0$$

From the local dissipation inequality and following the arguments presented by *Coleman and Gurtin, 1965*[10], we get the constitutive equations for Kirchoff stress tensor and entropy, almost same as in *Simo and Miehe, 1992*[13].

$$\boldsymbol{\tau} = 2\partial_{b^e}\psi\boldsymbol{b}^e \quad \text{and} \quad \eta = \eta^p - \partial_\theta\psi \tag{3.37}$$

Next, the values of $\mathcal{D}_{mech}$ and $\mathcal{D}_{ther}$ are deduced in the reduced form as was by *Simo and Miehe, 1992.*

3.2.5 Maximum plastic dissipation and flow rule

The elastic domain expression used here is same as of *Simo and Miehe, 1992.*

$$\mathbb{E} = \{(\boldsymbol{\tau},\boldsymbol{\beta},\boldsymbol{\theta}) : \boldsymbol{\phi}(\boldsymbol{\tau},\boldsymbol{\beta},\boldsymbol{\theta}) \leq 0\} \tag{3.38}$$

Also the same Von Mises yield criterion is considered(metal plasticity).

$$\boldsymbol{\phi}(\boldsymbol{\tau},\boldsymbol{\beta},\boldsymbol{\theta}) = \|\mathrm{dev}\,[\,\boldsymbol{\tau}\,]\| + \sqrt{\frac{2}{3}}\,[\boldsymbol{\beta} - \sigma_y(\boldsymbol{\theta})\,] \leq 0 \tag{3.39}$$

Using the principle of maximum plastic dissipation: from all admissible states $(\boldsymbol{\tau}^*,\boldsymbol{\beta}^*,\boldsymbol{\theta}^*)$ the plastic dissipation attains its maximum for the actual state$(\boldsymbol{\tau},\boldsymbol{\beta},\boldsymbol{\theta})$, they derived the following evolution equations:

$$-\frac{1}{2}\boldsymbol{\mathcal{L}}_v\boldsymbol{b}^e = \lambda\,[\partial_\tau\boldsymbol{\phi}\,]\boldsymbol{b}^e, \qquad \dot{\xi} = \lambda\partial_\beta\boldsymbol{\phi}\ , \qquad \dot{\eta}^p = \lambda\partial_\theta\boldsymbol{\phi}\ , \tag{3.40}$$

$$\lambda \geq 0\ , \qquad \boldsymbol{\phi}(\boldsymbol{\tau},\boldsymbol{\beta},\boldsymbol{\theta}) \leq 0\ , \qquad \lambda\boldsymbol{\phi}(\boldsymbol{\tau},\boldsymbol{\beta},\boldsymbol{\theta}) = 0 \tag{3.41}$$

and consistency condition,

$$\lambda\cdot\dot{\boldsymbol{\phi}}(\boldsymbol{\tau},\boldsymbol{\beta},\boldsymbol{\theta}) = 0 \tag{3.42}$$

3.2.6 Temperature evolution

Considering the energy balance equation of material, using the Piola transformation and taking Kirchoff stress tensor as a stress measure, the local energy balance can be written as,

$$-\boldsymbol{J} div\,[\boldsymbol{q}/\boldsymbol{J}\,] + r = \dot{e} - \boldsymbol{\tau}\cdot\boldsymbol{d} \tag{3.43}$$

Using the reduced dissipation inequality,

$$-\boldsymbol{J} div\,[\boldsymbol{q}/\boldsymbol{J}\,] + r = \boldsymbol{\theta}\dot{\eta} - \mathcal{D}_{loc} = \boldsymbol{\theta}(\dot{\eta} - \dot{\eta}^{p}) - \mathcal{D}_{mech} \tag{3.44}$$

By substituting the constitutive equation of entropy into the above equation, the temperature evolution can obtained as

$$c\dot{\boldsymbol{\theta}} = \,[\mathcal{D}_{mech} - \mathcal{H}\,] + \,[-\boldsymbol{J} div\,[\boldsymbol{q}/\boldsymbol{J}\,] + r\,] \tag{3.45}$$

The constitutive equation for heat flux for metal plasticity is always given by,

$$\boldsymbol{q} = -\boldsymbol{k}\nabla\boldsymbol{\theta} \tag{3.46}$$

3.2.7 Mechanical dissipation and structural elasto-plastic heating

There is a term of mechanical dissipation, $\mathcal{D}_{mech}$ in the temperature evolution equation which is usually defined by many authors as

$$\mathcal{D}_{mech} = \chi\mathcal{P}^{p}_{mech} = \sqrt{\frac{2}{3}}\,\lambda(\beta - \sigma_{y}(\theta)) \tag{3.47}$$

Where $\chi \in [0, 1\,]$ is a dissipation factor. Because, the mechanical power is mostly converted to thermal power and dissipated as heat and rising the temperature, but some of the mechanical power during plastic dissipation is left inside the material and stored due to the interaction of lattice structures, dislocations arrangements and many other micro-mechanics theories. The dissipation factor is usually taken as 0.85 to 0.95, but in some cases like *Rosakis et al., 2000*[32], this factor goes to 0.30 in certain cases. This stored amount of energy depends on many factors, strain rate, strain level, temperature, structural lattice etc. Considering the same free energy function, the elasto-plastic structural heating can be finally written as;

$$\mathcal{H} = -\theta(\partial^{2}_{\theta\bar{\boldsymbol{b}}^{e}}\boldsymbol{W}\partial_{\boldsymbol{b}^{e}}\cdot\dot{\bar{\boldsymbol{b}}}^{e} + \partial^{2}_{\theta J}\boldsymbol{U}\partial_{\boldsymbol{b}^{e}}J\cdot\dot{\boldsymbol{b}}^{e} + \partial^{2}_{\theta J}\boldsymbol{M}\partial_{\boldsymbol{b}^{e}}J\cdot\dot{\boldsymbol{b}}^{e}) \tag{3.48}$$

This is in accordance with the procedure adopted by *Rosakis et al.(2000).*

3.3 P. Wriggers, C. Miehe, M. Kleiber, and Simo; March, 1991

Introduction:

In the paper *P. Wriggers et al., 1991*[16], the same thermomechanical problem is discussed with isothermal, adiabatic and non-adiabatic case. It also showed that there is no bifurcation in the problem with heat flux as contrast to isothermal and adiabatic case. The same problem was also discussed by Oden for finite strains but for thermoelastic responses. The numerical formulation adopted by *P. Wriggers et al., 1991* is similar to that of developed by Simo[13], except the discussion on plastic incompressibility and incremental objectivity for thermomechanical problems.

3.3.1 Kinematic relations, multiplicative split

According to the multiplicative decomposition of the deformation gradient, *P. Wriggers et al., 1991* introduced the deformation gradient as

$$\boldsymbol{F} = \boldsymbol{F}_e \boldsymbol{F}_\theta \boldsymbol{F}_p \tag{3.49}$$

Where $\boldsymbol{F}_e$ is the deformation gradient by elastic contribution, $\boldsymbol{F}_\theta$ is the deformation gradient by thermal contribution and $\boldsymbol{F}_p$ by plastic contribution.
And splitting the $\boldsymbol{F}$ into volume preserving part $\hat{\boldsymbol{F}}$ and dilatoric part $J^{1/3}\mathbf{1}$.

$$\boldsymbol{F} = J^{1/3}\hat{\boldsymbol{F}} \quad \text{with} \quad det\,\hat{\boldsymbol{F}} = 1 \tag{3.50}$$

According to the classical plastic incompressibility and pure volumetric thermal deformations, $J_p = 1$, and $\hat{\boldsymbol{F}}_\theta = \mathbf{1}$, they get the following derivations.

$$J = J_e J_\theta \qquad \hat{\boldsymbol{F}} = \hat{F}_e \hat{\boldsymbol{F}}_p \tag{3.51}$$

$$\text{where} \quad \boldsymbol{F}_e = J_e^{1/3}\hat{\boldsymbol{F}}_e \quad , \quad \boldsymbol{F}_p = \hat{\boldsymbol{F}}_p \quad , \quad \boldsymbol{F}_\theta = J_\theta^{1/3}\mathbf{1} \tag{3.52}$$

Next the right Cauchy Green tensor $\boldsymbol{C}$ and elastic left Cauchy Green tensor $\boldsymbol{b}_e$ are then defined, finally the Lie derivative as

$$\boldsymbol{L}_v(\boldsymbol{b}_e) = \boldsymbol{F}\boldsymbol{C}_p^{-1}\boldsymbol{F}^T \tag{3.53}$$

3.3.2 Thermoelastic constitutive law

The free Helmholtz enegy introduced by *P. Wriggers et. al.*, is derivation from thermoelastic case and was written as

$$\psi(J_e, \hat{\boldsymbol{b}}_e, \theta) = \frac{1}{2}\mu(I_{\hat{b}_e} - 3) + \frac{1}{2}K(ln\,J_e)^2 + T(\theta) \tag{3.54}$$

And derived the constitutive equations for Kirchoff stresses and thermoelastic entropy quoting the paper *Thermoviscoplasticity by finite elements, by H. Ghoneim and S. Matsuoka, 1987* [22]:

$$\boldsymbol{\tau} = 2\boldsymbol{b}_e \frac{\partial \psi}{\partial \boldsymbol{b}_e} = -pI + \mu\, dev\,\hat{\boldsymbol{b}}_e \quad , \quad \eta_e = -\frac{\partial \psi}{\partial \theta} \tag{3.55}$$

The equations for change of volume due to thermal contribution (J_θ) and elastic deformation (J_e) are also given here.

3.3.3 Elastoplastic constitutive law

According to Von Mises yield criterion in terms of Kirchoff stresses:

$$f = \|\mathrm{dev}\,[\boldsymbol{\tau}\,]\| - \sqrt{\frac{2}{3}}\,\kappa(\alpha,\theta) \leq 0 \tag{3.56}$$

Here the strain hardening depends on hardening variable α, and thermal softening θ. The hardening-softening law is given as:

$$\kappa(\alpha,\theta) = \{Y_0 + (Y_\infty - Y_0)(1 - e^{-\delta\alpha}) + H_1\alpha\}\{1 - H_\theta(\theta - \theta_0)\} \tag{3.57}$$

Here the evolution of hardening variable is also given, and derived the flow rule same as by Simo et al.

$$\boldsymbol{L}_v(\hat{\boldsymbol{b}}_e) = -\frac{2}{3}\,\dot{\gamma} tr\,[\boldsymbol{b}_e\,]\boldsymbol{n} \quad \text{with} \quad \boldsymbol{n} = \frac{dev\,\boldsymbol{\tau}}{\|dev\,\boldsymbol{\tau}\|} \tag{3.58}$$

and consistency conditions,

$$\dot{\gamma} \geq 0\ , \qquad f(\boldsymbol{\tau},\alpha,\theta) \leq 0\ , \qquad \dot{\gamma} f(\boldsymbol{\tau},\alpha,\theta) = 0 \tag{3.59}$$

3.3.4 Balance laws and Variational formulation

In the current configuration, the local law of momentum for static case is written as

$$J\,div(\boldsymbol{\tau}/J) + \hat{\boldsymbol{b}} = 0 \tag{3.60}$$

The thermal effects were included by the balance of internal energy

$$\dot{\varepsilon} = \dot{w} - J\,div(\boldsymbol{h}/J) + r \tag{3.61}$$

where $\dot{\varepsilon}$ and $\dot{w}$ are the internal energy and total stress power. After neglecting the source term, r and the relatively small thermoelastic coupling effect, the temperature evolution equation is derived as:

$$c_e\dot{\theta} = \chi\dot{w}_p - J\,div(\boldsymbol{h}/J) \quad \text{with} \quad \dot{w}_p = \kappa(\alpha,\theta)\sqrt{\frac{2}{3}}\,\dot{\gamma} \tag{3.62}$$

Where c_e is the heat capacity, $c_e = \theta(\partial\eta_e/\partial\theta)$.

This is the coupled heat conduction equation for thermomechanical problems with heat dissipation. Here $\dot{w}_p$ is the plastic power and χ is the factor which indicates that how much plastic power is dissipated during plastic deformation. The term $-J\,div(\boldsymbol{h}/J)$ become zero in case of adiabatic. So the equation can be written without temperature term, simply as

$$\dot{\theta} = \frac{\chi}{c_e}\,\dot{\gamma} \tag{3.63}$$

But here, in *P. Wriggers et al., 1991* paper, they have ignored the thermoelastic coupling effect, so the expressions for plastic power $\dot{w}_p$, and temperature evolution equation are different than that of *Simo and Miehe- 1992,* because they have considered the effect of elastic thermal coupling. They introduced $\mathcal{H}$, as Elastic-plastic structural heating, and said that $\mathcal{H}$ is associated to the non-dissipative (latent) elastic and plastic structural changes.

In order to formulate the non-linear variational equations, it is said that the pure displacement approach is not being adopted due to isochoric nature of problem which may lead to locking. They consider a five field mixed formulation consistent with thermomechanical problem. The momentum balance equation and the temperature evolution equation are formulated with Galerkin formulation, with the test functions $\boldsymbol{\eta}_u$ and $\boldsymbol{\eta}_\theta$ respectively and finally formulated the following functionals.

$$G_\phi = \int_\Omega [dev\,\boldsymbol{\tau} \cdot dev\,(\nabla \boldsymbol{\eta}_u) - P\,\nabla \cdot \boldsymbol{\eta}_u\,]dV - \int_\Omega \hat{\boldsymbol{b}} \cdot \boldsymbol{\eta}_u dV - \int_{\partial_\tau \phi(\Omega)} \hat{\boldsymbol{t}} \cdot \boldsymbol{\eta}_u da = 0 \tag{3.64}$$

$$G_D = \int_\Omega (D - J)\eta_D\, dV = 0 \tag{3.65}$$

$$G_T = \int_\Omega (T - \theta)\eta_T\, dV = 0 \tag{3.66}$$

$$G_P = \int_\Omega [P - K\, ln\,(D\, e^{-3\alpha(T-\theta_0)})\,]\eta_p dV = 0 \tag{3.67}$$

$$G_\theta = \int_\Omega [c_e \dot{\theta}\eta_\theta - \boldsymbol{h} \cdot \nabla \eta_\theta - \chi \dot{w}_p \eta_\theta\,]dV - \int_{\partial_q \phi(\Omega)} (-\hat{q}_n)\eta_\theta\, da = 0 \tag{3.68}$$

And detailed the effect of plastic dissipation on temperature, influence of deformation on heat generation, and the change of stress behavior due to rise of temperature.

Part II

Computational Experiments and Comparison

Chapter 4

Results from Abaqus Simulations

Here in the current chapter, the problem will be defined completely along with a brief history of the specific problem. The computational procedure via Abaqus will be discussed in detail, step by step. After the discussion of the Abaqus Procedure of tackling plasticity problems, the results will be presented. The results include the comparison of temperature distribution, load distribution, stress-strain curves, and reduction of the diameter during necking process.

Thermally triggered necking; A classical thermomechanical test case:

The necking problem is one of the very known cases for verification of the studies and numerical formulations developed in the field of thermomechanical plasticity, dealing with isothermal, adiabatic and non-adiabatic cases. This is the standard size cylindrical bar of radius 6.413 mm and length of 53.334 mm. The total axial elongation of the specimen is prescribed to be 16 mm. The total time period is 8 seconds, and the rate of application of the stretching is kept constant. The cylindrical bar has the properties detailed in table 1. The similar problem was dealt by many of the authors, including *Needleman, 1972*[25], *Lehmann and U. Blix, 1985*[24], *T.J.R Hughes et al., 1983*[28], *H. Ghoneim and S. Matsuoka, 1987*[22], *P. Wriggers et al. 1992*[16], *F. Armero et al. 1992*[12], *J.H. Argyris, J.S. Doltsinis,1979*[19], *J.C. Simo and C. Miehe, 1992*[13], *Marko Canadija and Josip Brnic, 2003*[29], *A. Ibrahimbegovic and L. Chorfi, 2002*[30], *Q. Yang, L. Stainier, and M.Ortiz, 2006*[14] etc. are the most prominent scientists in the field of computational thermo-plasticity. First of all, the problem was dealt with simple plasticity, i.e. plasticity without the conversion of plastic power in thermal power raising the temperature in the material. Then later on, the same problem was dealt in context of non-isothermal but with adiabatic surface and with bifurcations. Afterward the problem was studied with heat conduction but in context of isotropic hardening only by some of the authors.

The work in *Simo and Miehe, 1992*[13] proved to be an excellent bench mark in thermomechanical plasticity, both in governing equations and computational formulations. Seven representative examples were studied and explained with the computational formulations by *Simo and Miehe, 1992*[13]. The results of these seven examples were regarded as refer-

ence work for many of the authors later on. Their work for metal plasticity got the status of reference for other disciplines, like composite materials, porous materials, temperature dependent material properties, thermoplasticity with kinematic hardening only, thermoplasticity with isomorphism, thermoplasticity with both kinematic and isotropic hardening (e.g. *A. Ibrahimbegovic and L. Chorfi, 2002*[30] and for Aluminium by *Q. Yang, L. Stainier, M. Ortiz, 2006*[14] and by many others). . One point to note that, the case dealt by *Simo and Miehe, 1992*[13] is the isotropic hardening case only, with constant material properties. The temperature-dependent material properties are detailed in the work by *Marko Canadija and Josip Brnic, 2003*[29].

Here, the problem is studied from three perspectives.First the theoretical study of the laws of mechanics and thermodynamics are studied from many of the internationally renowned papers and from the books as are detailed in bibliography. These laws include the equations of kinematics, mass balance, momentum balance, constitutive, energy, entropy, temperature evolution, entropy evolution, and plastic flow equations. Secondly, the problem was carried through Abaqus formulations of numerical coding. Many of the parameters, e.g. mesh size, strain rate, load rate, coefficient of convective heat, temperature variation, necking zone radius, material properties, stresses, strains and computational time were observed. Thirdly, the problem was tested in the code, Zorglib developed by *Prof. Dr. Laurent Stainier*. Here in this part, the GMSH was used along with the python script, input files of material properties and mesh. The GMSH is software used for meshing and post processing, it is an open source code provided by GNU General Public License.

4.1 Excution Detail in Abaqus

The given sample for tensile test is a cylindrical shape bar of radius 6.413 mm and length 53.334 mm discussed by in [13]. The specific problem of thermal necking in a cylindrical bar is investigated by many of the authors. The problem is detailed first as an isothermal case by Needleman[**?**], Argyris and Doltsins [19][18], and Simo [27]. The same problem with same geometry is also discussed as non-isothermal (adiabatic problem) by *T. Lehmann and U. Blix, 1972*[24]. Recently the same problem with self heat generation and convection (convective problem) with the same geometry is discussed by [13], [29], [31] and [30]. The sample considered here has axisymmetric conditions; One-quarter of the specimen is taken. So the 2D shape of the specimen can have only Quadrilateral and Triangular elements and it can be of order 1 and 2 only, in other words, we can have only linear and quadratic quadrilateral elements and triangular elements. Here the main steps of Abaqus are discussed.

4.1.1 Properties of Material

The table (4.1) shows the properties of the necking problem considered here. The properties taken by other authors for the same geometry are mostly the same. There are very little changes in the properties, e.g. thermal conductivity, coefficient of convection heat, and some

Table 4.1: Material properties for thermally triggered necking

Bulk modulus	κ	164206	N/mm^2
Shear modulus	μ	801938	N/mm^2
Flow stress	y_o	450	N/mm^2
Linear hardening	h	129.24	N/mm^2
Saturation hardening	$y_{o,\infty}$	715	N/mm^2
Hardening exponent	δ	16.93	
Density	ρ	$7.8 \cdot 10^{-9}$	Ns^2/mm^4
Expansion coefficient	α	$1{\cdot}10^{-5}$	K^{-1}
Conductivity	κ	45	N/sK
Capacity	c	$0.46 \cdot 10^9$	mm^2/s^2K
Dissipation factor	χ	0.9	
Flow stress softening	ω_o	0.002	K^{-1}
Hardening softening	ω_h	0.002	K^{-1}

[b)] Values taken from Simo and Miehe, 1992

other constants, of other authors who worked on the necking problem, and those changes does not count much in the general results. Here in the current Abaqus simulation, the mechanical properties of the specimen is taken at constant temperature, in other words, the properties are independent of the temperature. The analysis become more complex if one take the temperature dependent properties.

4.1.2 Plastic Strain Data

Similarly, the plastic strain data introduced in Abaqus simulation is given in the table (4.2). The plastic strain data is taken from the analytical expression from Simo and Miehe, 1992 paper. The plastic strain data is taken at two different temperatures. This is the experimental data used in the Abaqus computational simulations.

4.1.3 Analysis step

Here in the Step, the values and observation found are explained for one of the many cases performed. The case is 200 quadrilateral element with first order of shape functions. A standard structured mesh with thermocoupled temperature displacement element was set. Time period was set to 8 sec, with Nlgeo on, initial increment size as 0.02, minimum increment 8e-5 and maximum increment size 0.02. Allowable temperature change per increment was set to 10. The analysis stopped at 405th increment while the total number of increments were given 1000. The computational time was almost 3 minutes. The necking started at 148th increment when the Avg Mises Stress at the bottom of the bar, at 145th increment changed from 6.735e8 Pa to 6.594e8 Pa at 148th increment. But there was one region (blue) with 5.493e8 Pa in the middle of the bar on the axis of symmetry, still in these increments.

Table 4.2: Experimental data for thermally triggered necking

Plastic strain data		
Yield stress(MPa)	Plastic strain	Temperature(K)
450	0	0
520	0.02	0
580	0.04	0
640	0.08	0
700	0.15	0
780	0.5	0
840	1	0
270	0	200
312	0.02	200
348	0.04	200
384	0.08	200
420	0.15	200
468	0.5	200
504	1	200

[c)]Experimental data for medium carbon steel

At 200th increment the stress on these bottom elements decreased to 5.847e8 Pa along with the blue region at 2.824e8 Pa, but shifted and spread towards bottom. At 300th, 350th and 400th increment, the stresses at the bottom of the bar were noted as 5.361e8 Pa, 4.065e8 Pa and 5.435e8 Pa.

4.1.4 Interaction

Interaction of type Surface Film Condition with Film Coefficient 17.5 N/msK , Skin Temperature, 0, with respect to the reference temperature taken as outside temperature, is created in step 1 which is a Coupled Temperature Displacement step. In the Interaction Property, the Film Coefficient is 17.5 N/msK at Temp 0. In Abaqus, first it needs to define type of interaction, and then for each interaction type there are some interaction properties. Here, the upper and right line of 2D rectangular axisymmetric specimen was given the interaction with surrounding for heat transfer. So one can observe the temperature difference for the elements on the line of symmetry and on right line elements. The temperature on axisymmetric line is always greater than that of right line elements.

4.1.5 Load and Boundary Conditions

BC1, BC2 and BC3 are created in step 1 (Coupled Temperature Displacement), BC1 and BC2 are of type Symmetry/Antisymmetry/ncastre, while BC3 is of type Displacement/Rotation. BC1 and BC2 are XSYMM and YSYMM. BC3 is given a displacement of 8 m only to U2, in other words, a velocity of 1mm/s was given to the upper end of the specimen. This

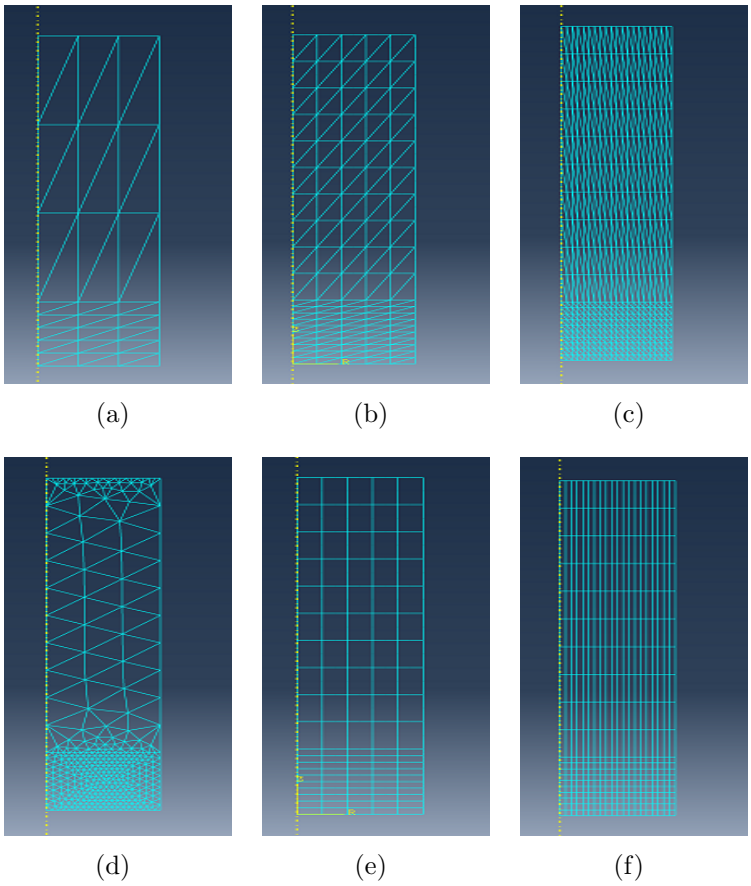

Figure 4.1: The various forms of meshes for different test cases

step is very crucial because varying the time step vary the results unexpectedly most of the time.

4.1.6 Mesh

The Figure (4.1) represents the different sizes of meshes. The mesh can be structured or free. The specimen is divided into two parts, the upper part and the lower part. The lower part is the necking zone, which is concentrated with more number of elements with respect to the upper part for the convergence of results. As the case is axisymmetric, so it can be assigned only two dimensional elements, which can be triangular or quadrilateral. The order can be changed to first and second, with type of mesh, number of elements, time increment, convection heat coefficient, time of applied load, properties of the material etc.

Case 1:

In Mesh Control the element shape is Quadrilateral and is structured. In the Element Type, the family is Coupled Temperature Displacement, standard, and the geometric order is linear. In other words, the elements are CAX4T (4 node axisymmetric thermally coupled quadrilateral, bilinear displacement and temperature). Here is the partitioning in the necking region. There are 100 elements in the necking region and 150 elements in the upper region, the calculations completed at 405 elements. There were some problems, first, when the mesh was not structured, it shows the necking in between the bar not at the end, and such behavior was unexpected and the analysis stopped at almost the same number of increments, 402 in this case. Similarly when the elements were structured, but the number of elements in the bottom was increased from 100 to 200 and the upper region elements were increased from 150 to 200 elements, then the results showed necking at both ends of the bar. These were weird results. In one another attempt, when the upper elements changed to 160 and the lower elements were remained same, it showed necking in the center of the bar even this time the mesh was structured. In the 4th attempt, the number of elements lower region kept 200 same, but changed the width to length and vice versa, and the upper part was kept same at 150 elements. This time it gave the error of excessive distortion.

Case 2:

After that, the time step was changed and the initial increment was made to 0.01s and the maximum increment was also changed to 0.01s. The lengths of the specimen were changed to meters. This time the analysis completed at 806th increment, necking only at the bottom, the blue region shifted to above a little and then came back at the same location, and the computational time was increased from 3 min to 10 min and the necking started at 707th increment with 6.254e8 Pa at the bottom elements instead of 148th increment with 100 elements on bottom and 150 elements in upper region. The Avg. Mises stress at 804th increment was almost the same as was observed with case of 100 and 150 elements bar (5.201e8 Pa) at bottom elements.

4.1.7 Job

The Job module comes after the completion of all graphics, properties of materials, interactions, boundary conditions and loading conditions and finally meshing. After all the requirements for the job are completed, then the problem is called a job and is given a name which defines the type and nature of job. The job is then submitted for solution. The monitor window is then opened to observe all the steps one by one. One can observe the log file, data file, dot file to look at the errors and warnings during the execution of job.

4.1.8 Results

The results stage of the Abaqus comes after the execution of job, it is called as post processing. Here the Abaqus has a large variety of results. In Abaqus,there is one very helpful feature, Operate on data, which help to make any mathematical operation on data. One can operate on the data mathematically and there are a lot of mathematical operations one can do just with one click. But it also sometime create complexity and ambiguity of results if one is not familiar with all those result measures, for example there are many measures of strains, stress, displacements, and load and various point of interest. So, the bearer of the undergoing thesis tried to explain the results with the help of options given in Abaqus. These specific details are mentioned in appendix B only for the current problem of necking.

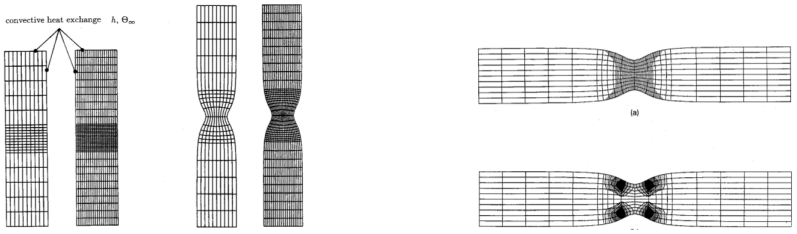

(a) Undeformed Shape (b) Deformed Shape

Figure 4.2: Simo and Miehe test cases of 50 and 200 quadrilateral elements

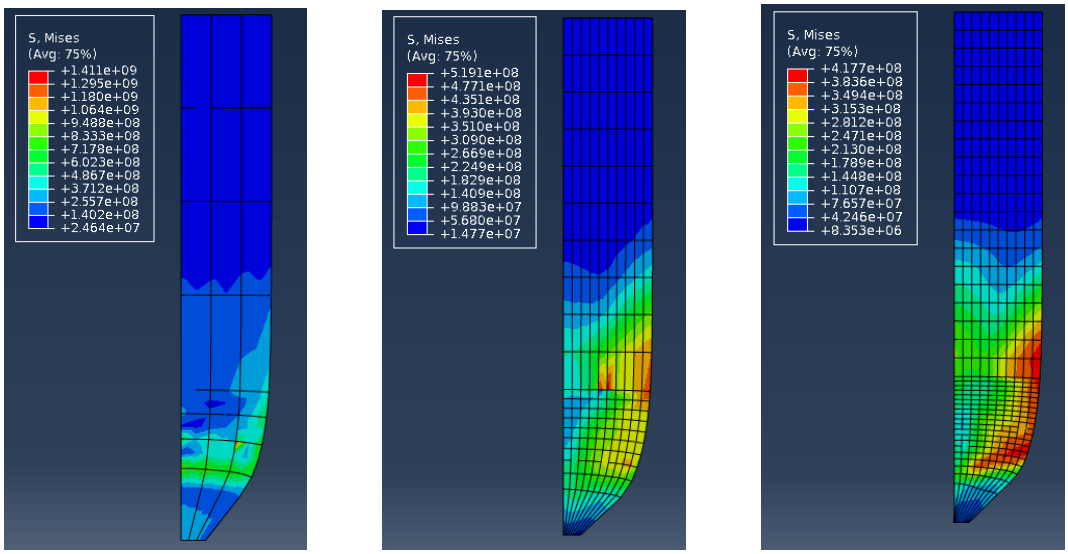

(a) The 24-element Quadrilaterals (b) The 200-element Quadrilateral (c) The 400-element Quadrilateral

Figure 4.3: Various size of Quadrilateral Elements in their Necking

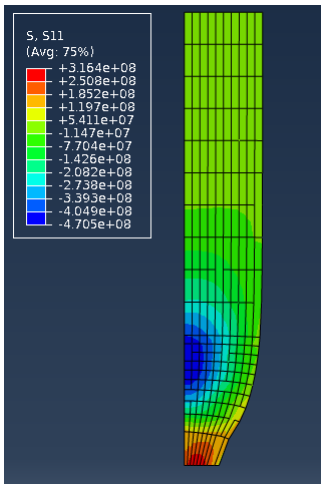

(a) Abaqus Contour Plot

(b) Lin and Brocks Contour Plot

Figure 4.4: S11 Contour Plot Comparison

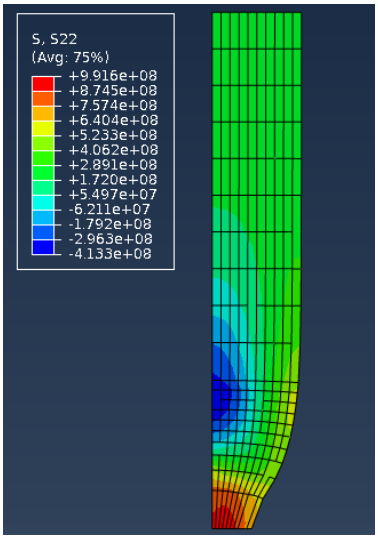

(a) Abaqus Contour Plot

(b) Lin and Brocks Contour Plot

Figure 4.5: S22 Contour Plot Comparison

In the Figure (4.11), a mesh of 200 quadrilateral elements of coupled temperature displacement with first order, from standard library were taken to test the necking problem with temperature dependent material properties. The properties were taken at the average temperature of 323K and 373K. The maximum temperature change was about 125 as compared to the change of 115 in constant material properties. The graph (b) of the same figure shows that the rise decreased to 120 with material properties dependent at temperature of

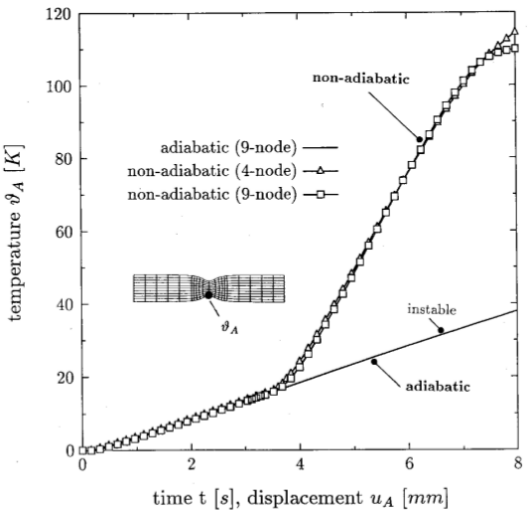

(a) Simo-Miehe Temperature Distribution

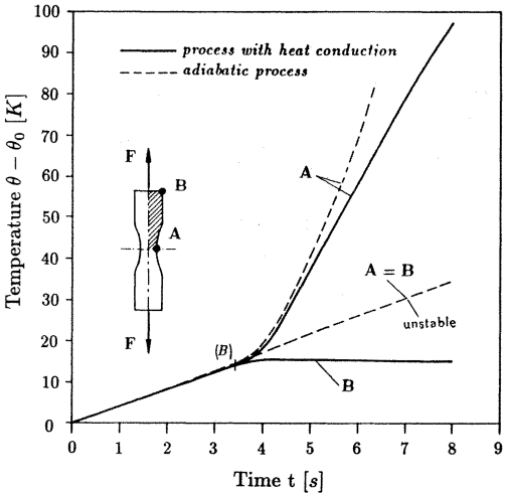

(b) Wriggers Temperature Distribution

Figure 4.6: Simo-Miehe and Wriggers cases for adiabatic and non-adiabatic temperature distribution

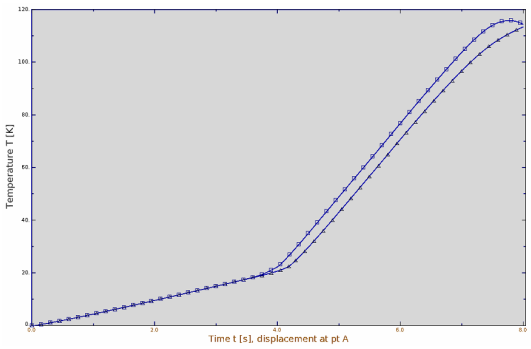

(a) Quadrialateral elements order 1 and 2

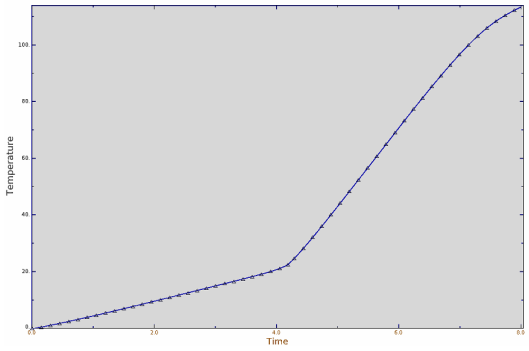

(b) Triangular elements of order 1 and 2

Figure 4.7: Abaqus cases for adiabatic and non-adiabatic temperature distribution

average 373K. The case in *Canadija and Brnic* [29], is different. It shows a high temperature change of about 160, and moreover the slope of the graph at the end of necking is still too high contrary to the graph of constant material properties, as the case in *Simo and Miehe, 1992* [13]. During the simulation process and from Newton Raphson method, it evident that the time increment plays an important role during the calculations of non-linear equations. Here in the specific case, the outcome as a result of too high increment reveals the unstability of the necking process. Sometimes it becomes difficult to judge, whether it came from bifurcation or high time increment. Due to the crucial nature of time step in the whole simulation, it is better to get good result on the expense of large computational time. The number of time increment was taken high and the initial time time step was taken very low. The details of some simulation result were written precisely in detail in the beginning of the

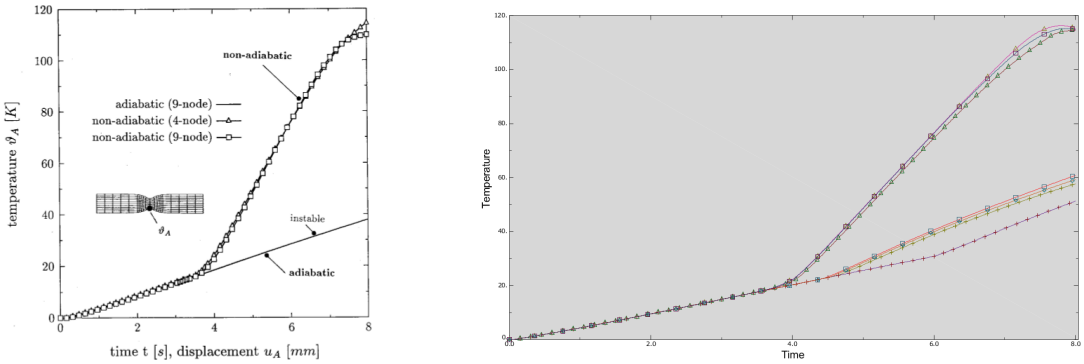

(a) Simo-Miehe Temperature Distribution

(b) Abaqus results

Figure 4.8: Abaqus cases for adiabatic and non-adiabatic temperature distribution

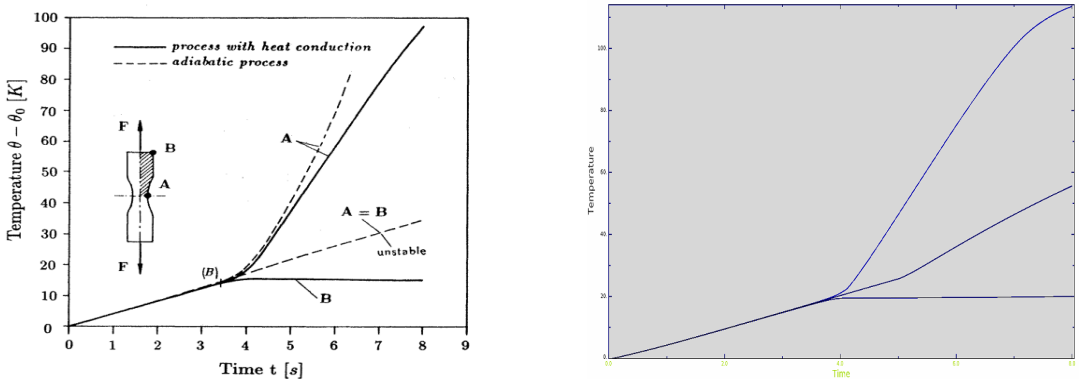

(a) P. Wriggers Temperature Distribution

(b) Abaqus results

Figure 4.9: Comparison for adiabatic and non-adiabatic temperature distribution

current chapter. The Newton Raphson method was given with more options in Abaqus, as it can choose between minimum time increment and maximum time increment starting from initial time increment. The number of iterations per increment are defined earlier in order to abort the simulations in case of divergence of results.
So, in order to verify the effect of total time, the time in the simulation results were reduced to 6 seconds and 7 seconds successively. Evident from the the Figure (4.12) , it reveals that the necking time started earlier and the temperature increment is also higher. The end slope of the line is almost same as before indicating the gradual decrease of high temperature increment after the setting of crystal lattice layers movement initiated by necking.

The inelastic heat fraction factor is taken as constant for metal plasticity. It is usually taken as $\chi\,[0.85 - 0.95\,]$ for metal plasticity. In fact it shows the dissipation of plastic power into thermal power, in other words it is the fraction of plastic work dissipated into heat. It is detailed by *Cervera et al. (1999), Zdebel and Lehmann(1987), Kamlah and Haupt (1998)* and *Rosakis et al. (2000)*. The *Rosakis et al. (2000)* [32], presents that the factor can

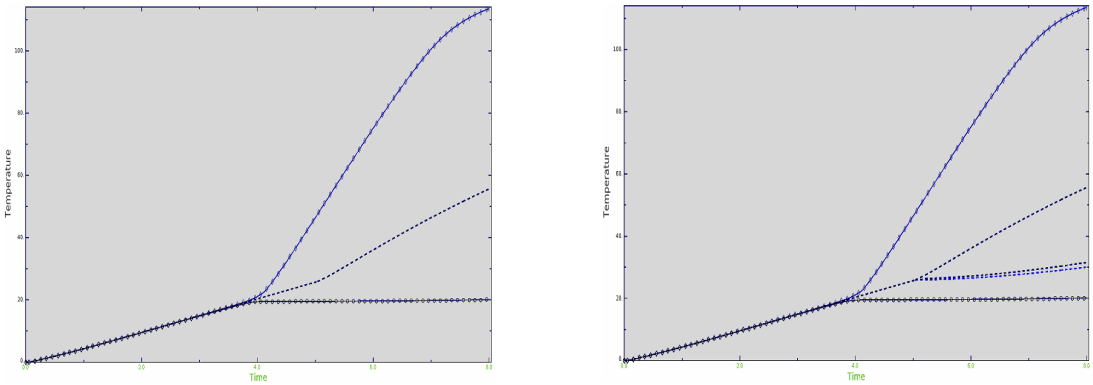

(a) Temperature Distribution (b) Birfurcation in adiabatic lines

Figure 4.10: Bifurcation of adiabatic temperature distribution

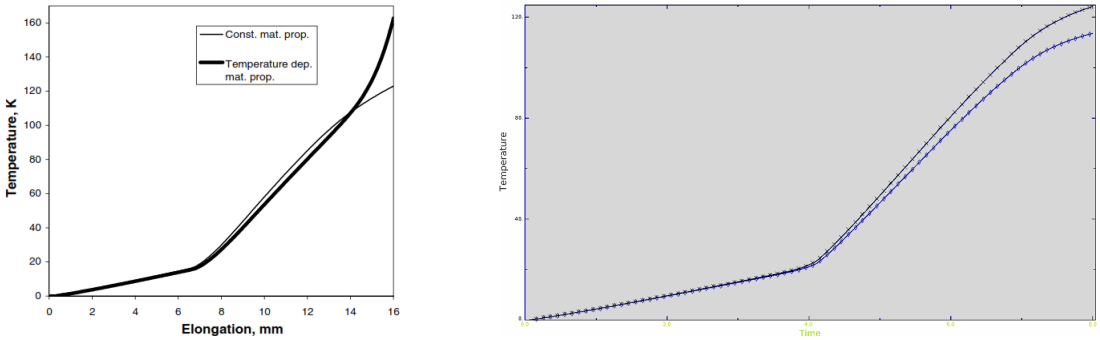

(a) Canadija-Brnic Temperature Distribution (b) Abaqus results

Figure 4.11: Temperature dependent data; Comparison

reach to a value of 0.30 in some materials.
Here the effect of the dissipation factor shows the drop of temperature change successively by lowering the value of dissipation factor. In Figure (4.13), the graphs for values of 0.9 (blue), 0.8, 0.7 and 0.5 are taken. At dissipation factor of value 0.5, the problem show unstability and the necking starts at different positions. Since the convection coefficient is highly dependent on the velocity of the convective medium, air in the case of necking. Here the convection coefficient was doubled and then tripled, but there was negligible change in the graph as shown in the Figure (4.14).This area need more realistic approach in numerical implementations. Here in the Figure (4.16), the two lines shows the temperature at the right of specimen (outside periphery) and left side (on the center line of specimen). The upper line in both the graphs shows the temperature on the element which lie in the necking zone and on the line of symmetry. It has slightly more temperature which is due to the lack of convection heat transfer on the center line of the specimen. But there is difference between these two graphs when we perform the reduced integration, which saves little time

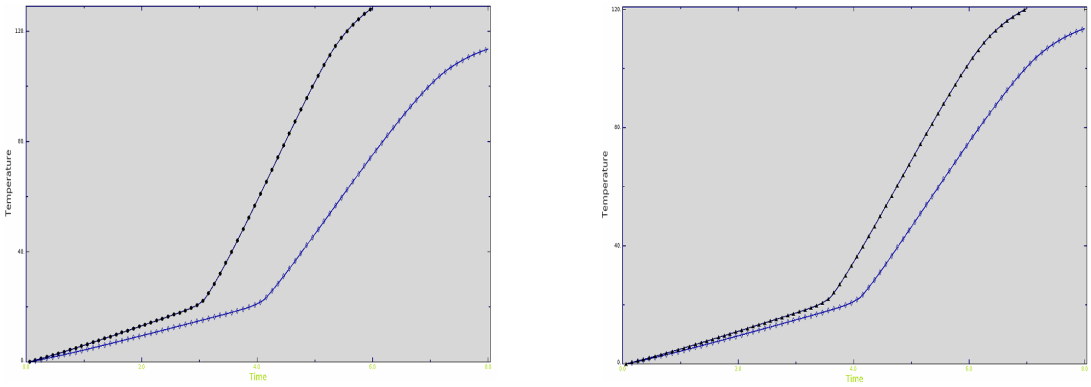

(a) Temperature Distribution t= 6 sec (b) Temperature Distribution t= 7 sec

Figure 4.12: Effect of time increment on temperature distribution

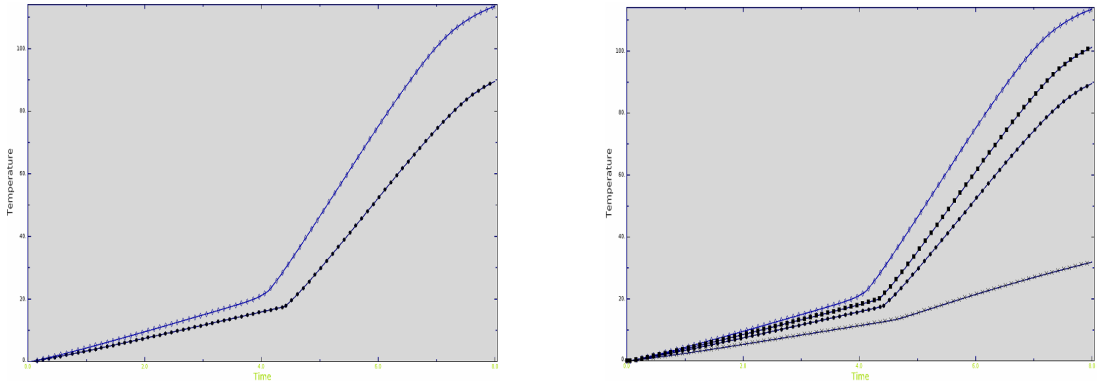

(a) Dissipation factor of 0.9 and 0.7 (b) Varying dissipation factors (0.9, 0.8, 0.7, 0.5)

Figure 4.13: Temperature distribution under varying dissipation factor

in the current sample problem, but it shows some difference of curves mainly at the end of necking.

The Figure (4.17) and shows the various possibilities of the unstability conditions. Here due necking starts at the upper end of the bar and similarly at the center of the bar. It may be due to bifurcations, adiabatic conditions, improper meshing, unstable time increment, reduced integration for a mesh of less elements, isothermal conditions, improper element type or unsuitable strain rate.

Similarly Figure (4.19) shows the unstability in the triangular elements. In addition to the very less number of the elements in the mesh, the the type of mesh is structured. For the specific, when the mesh made of free, then it shows stability of necking zone for suitable number of elements.

There are various kinds of measures for stress-strain graph. Here, only the Figure (4.20)

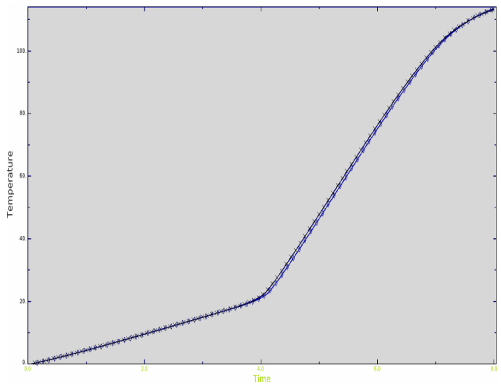

(a) Conv. coeff; Two times the origional value

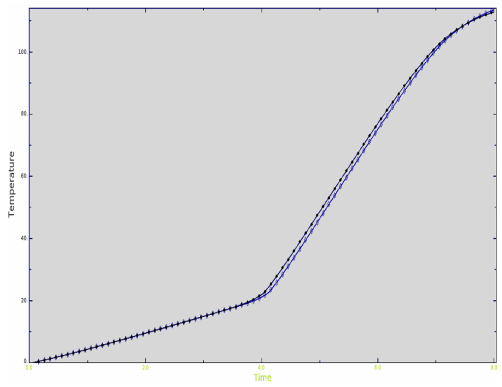

(b) Conv. coeff; Three times the origional value

Figure 4.14: Temperature distribution with higher convective coefficients

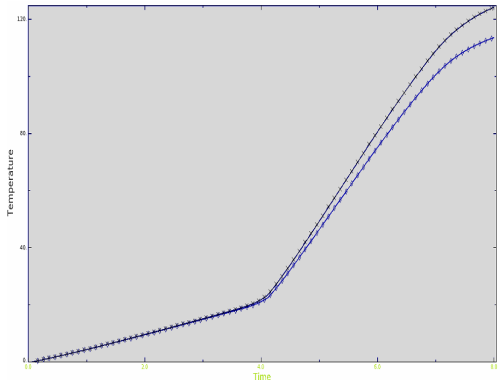

(a) Properties at aveg. tempe. 323K

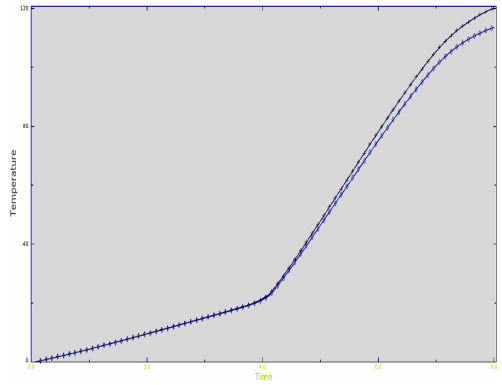

(b) Properties at aveg. tempe. 373K

Figure 4.15: Temperature dependent material properties;Comparison

is explained. It is stress-strain graph for LE, Logrithmic strain components LE22 (vertical direction) at the integration points of each element, here the element is 4 node, and the integration points are 4, so we have 4 strain-time graphs for each element and 4 stress-time graphs, but here is given only one graph for strain, and one for stress, and one by then combining these two graphs, for each element. The element considered here is on the bottom line along the symmetric side where the necking was developed.

Here first of all, the results at integration points are taken, which includes the stress-time, strain-time, and the stress-strain graphs. One point to clear, the strain component is LEE, it is logarithmic strain, while the stress component is S22. We have four data for four intregration points of the node, the node is at the bottom left of the specimen. The strain here is the logarithmic strain at one of the integration point.

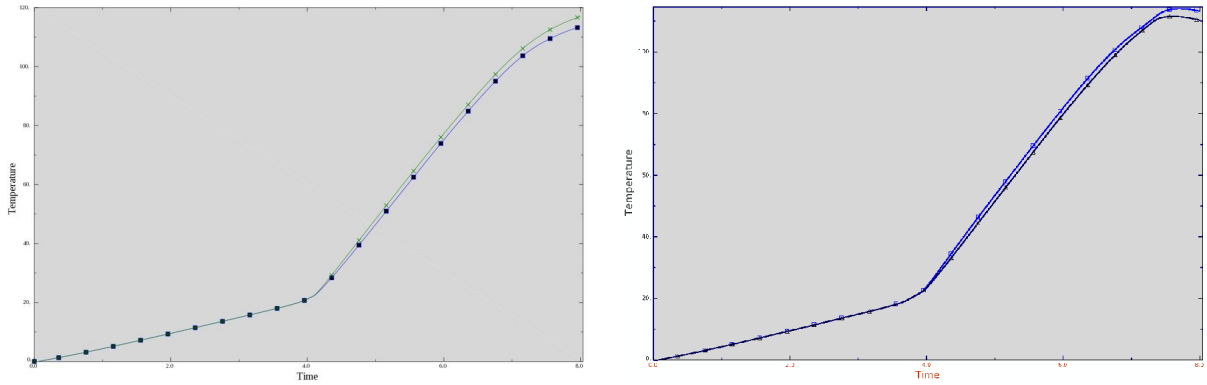

(a) Convection with Full Integration (b) Convection with Reduced Integration

Figure 4.16: Quadrilateral Elements with 200 Elements

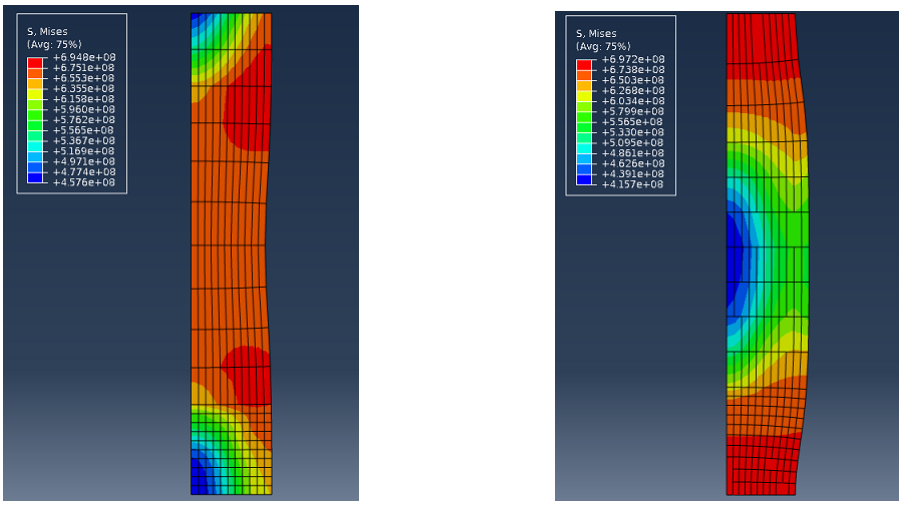

(a) Displacements of all nodes (b) Displacement of midpoint in time

Figure 4.17: Unstability due to Adabatic Case

The Figure (4.20) shows the stress strain graph for LE, Logrithmic strain components LE22 and stress component S22. The measurement is taken at integration points of each element; Here the element is 4 node, quadrilateral and the integration points are 4, so we have four strain-time graphs for each element. Similarly four stress-time graphs for each element. The elements considered here are on line along the symmetric side and on outer periphery where the necking was developed.By combining the two graphs of strain-time and stress-time at any of the integration point we get the stress-strain graph for that specific integration point. Here the values of strain are logrithmic, and mostly we have nominal values in stress-strain graphs.

Similarly in Figure (4.24), the temperature distribution at the elements on the right

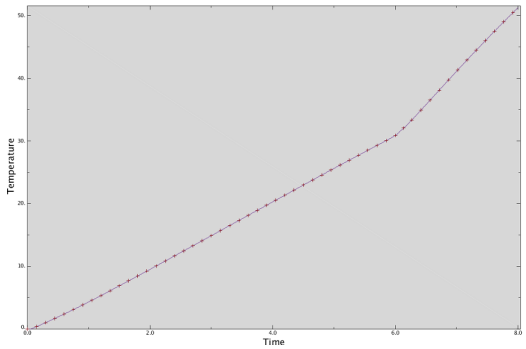

(a) Quadrilateral elements with full integration

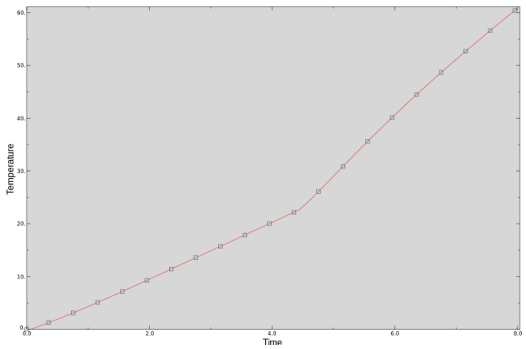

(b) Quadrilateral elements with reduced integration

Figure 4.18: Unstability of Adabatic Case

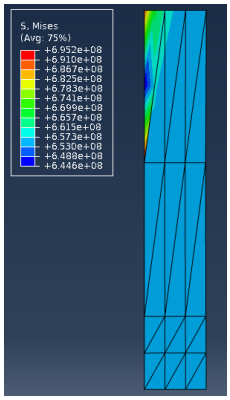

(a) Unstability with structured Meshing

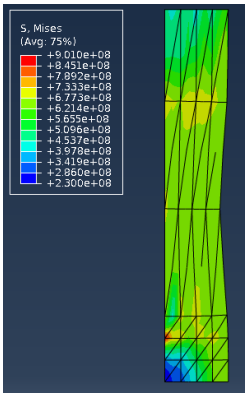

(b) Unstability with free Meshing

Figure 4.19: Triangular element adiabatic case

edge of the specimen are investigated for the value of convection heat values at normal temperature and at the value of 293 K.

The Figure (**??**) represents the load-time graph for quadrilateral elements with free meshing techniques. For the case of *Simo and Miehe* [13] the values are taken for one element on the top. In other papers, the values are added for all the elements on the top of the specimen and results in the value ranging between 70 to 100 KN after the elastic range.

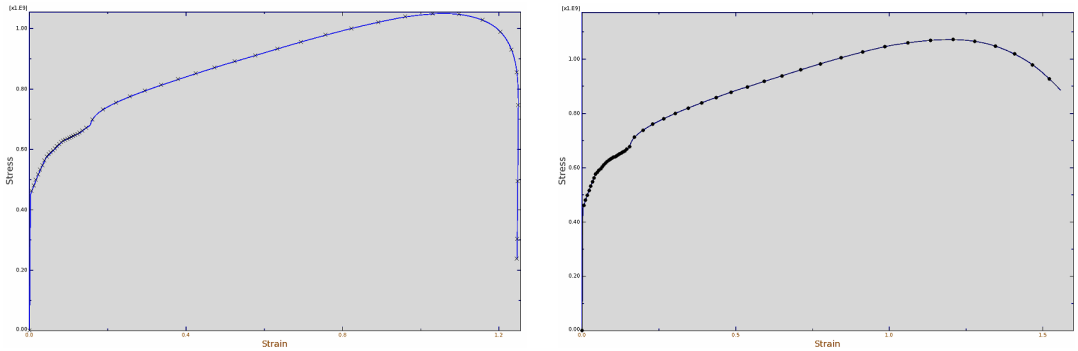

(a) Element on top (b) Element on bottom

Figure 4.20: Stress-strain diagram: logrithmic strain component LE22 and stress component S22

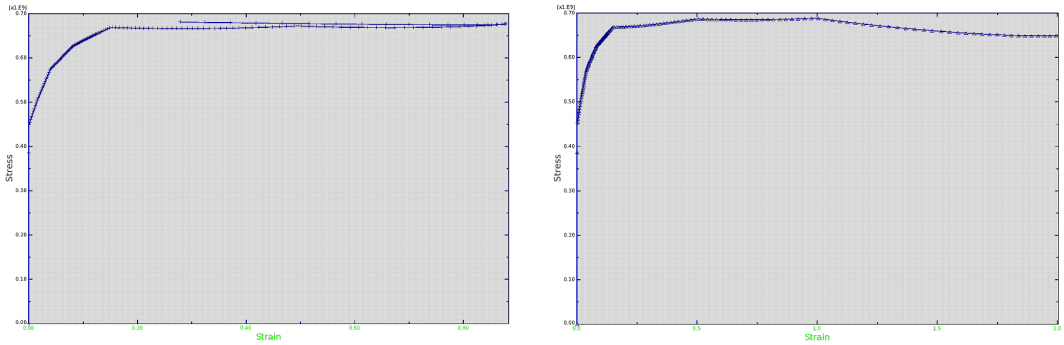

(a) Stress-strain on outer periphery node (b) Stress-strain on the symmetric axis node

Figure 4.21: Stress-strain diagram: Equivalent plastic strain component PEEQ and Mises stresses

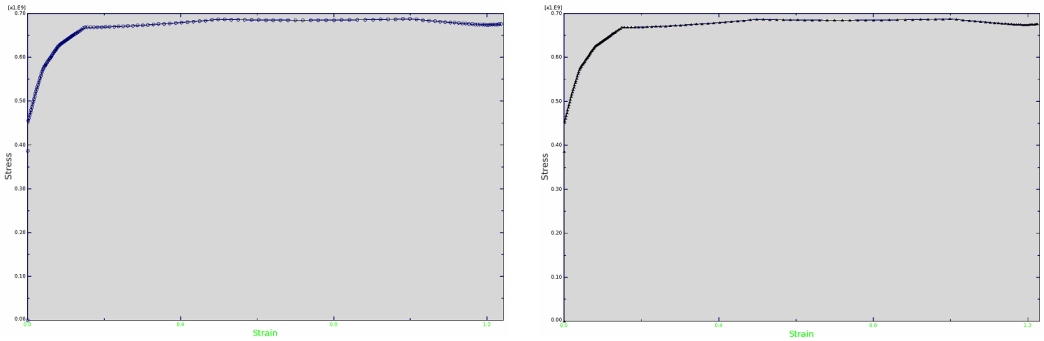

(a) Magnitude of plastic strain, PEMAG (b) Plastic strain, PE22

Figure 4.22: Stress-strain: Quadrilateral 8 node element with Mises stresses

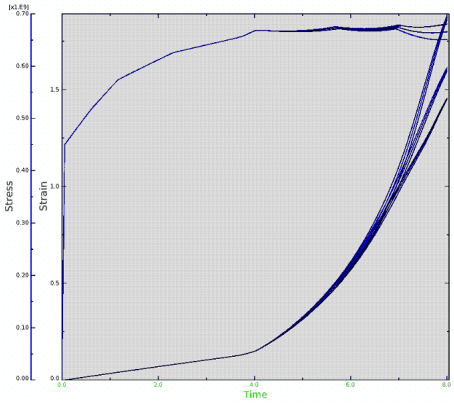

(a) PEEQ and Mises stress with 8-node element

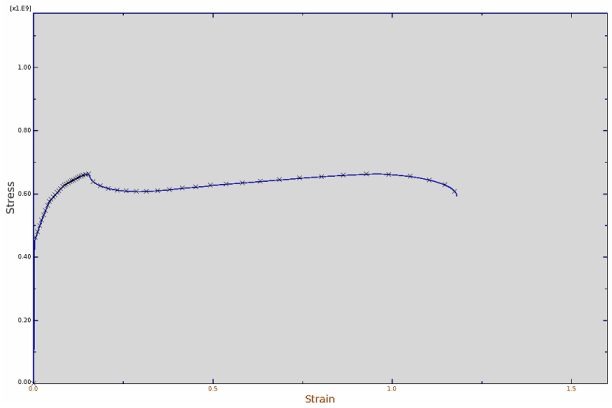

(b) LE22 with 4-node element and S22

Figure 4.23: Stress-strain: Quadrilateral elements on the right

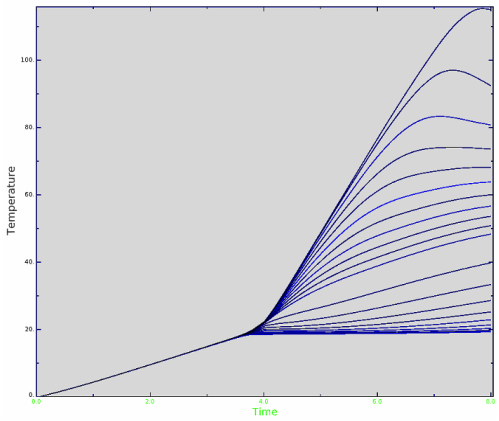

(a) With Convection Coeff. by Simo and Miehe

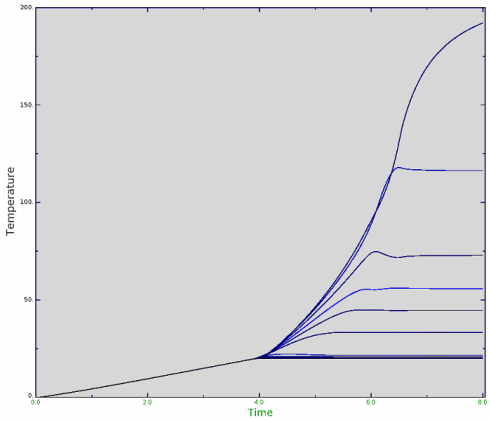

(b) With Convection Coeff. of Higher Value

Figure 4.24: Temperature distribution of all nodes on periphery during necking

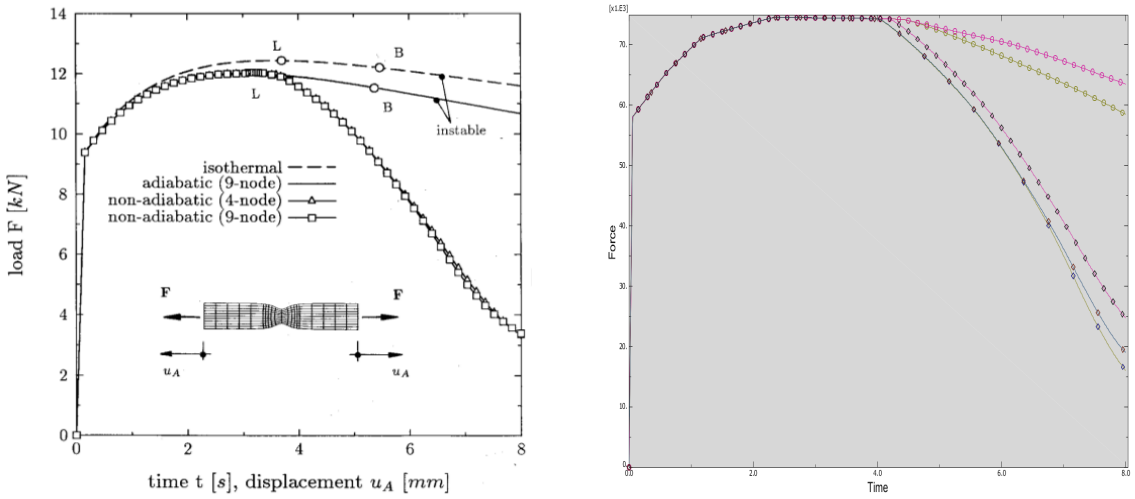

(a) Simo and Miehe Load Distribution (b) Load Distribution

Figure 4.25: Comparison of load-time graph

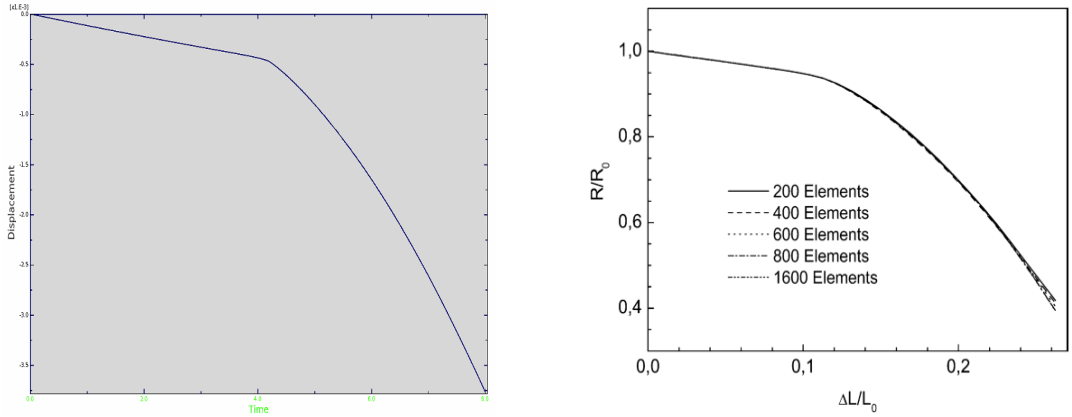

(a) Abaqus Results (b) Lin and Brocks Results

Figure 4.26: Radius and Length Ratio During Necking

The Figure (4.28) shows the vertical and horizontal displacements of the nodes on the right line of the axisymmetric two dimensional geometry considered here. There is very evident difference in the behavior of nodes just before and after necking which start just after 4th second in most of the cases in Abaqus. One can observe in the Figure (4.28a), the elements near the necking zone have very less vertical displacement in the start and it just increased exponentially after the start of necking. This behavior makes the necking phenomenon as a unique case to study in the tensile behavior. Such behavior is also clear from Figure (4.28b) for the horizontal displacement where the elements near the necking zone has sudden increase of horizontal displacement resulting in the reduction of diameter at necking zone specifically.

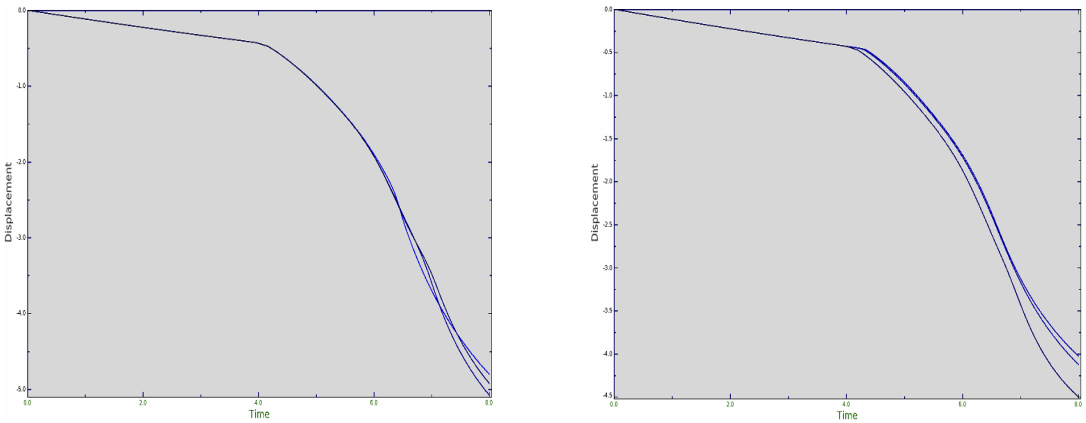

(a) Quadrilateral elements (b) Triangular elements

Figure 4.27: Abaqus: Radius and Length Ratio During Necking

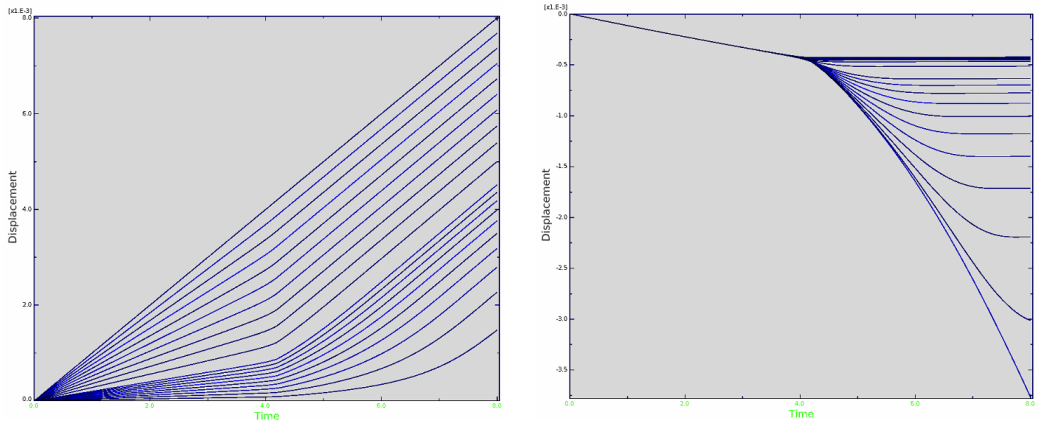

(a) Vertical displacement (b) Horizontal displacement

Figure 4.28: Displacement of all nodes on periphery during Necking

4.2 Tables of Observations

The simulations for the first order triangular elements are non-linear and they have unexpected behavior of necking at different values of mesh size, step time increment, initial increment size and varying velocity applied to the end of the bar. The specimen shows the necking at different location of the of bar, for example with less number of elements it shows the necking at both the upper and lower sides of the symmetric portion. Similarly with high number of elements it shows the necking at center which is not the case in actual experimental cases. Sometime, by changing the mesh control values, like making it as free mesh instead of structured one, it change the behavior. So an unstable case is unpredictable by varying the parameters. So, the graph for CAX3T (linear three node triangular elements) is not fruitful to take into considerations.

Table 4.3: Abaqus Results for CAX4T element

Case No.	No. of Elements	Comp. Time (hr:min:sec)	Necking Start Radius (mm)	Final Rad. (mm)	Necking Start Time (mm)	Final Tempe. (^{o}C).
1	24	00:01:08	5.815	3.023	Unstable	42
2	50	00:01:43	6.010	2.713.	4.10	109
3	100	00:02:25	6.013	2.631	4.15	109.50
4	200	00:04:42	6.015	2.511	4.28	110.0
5	400	00:06:01	6.015	2.500	4.30	111.0

[a)](All the values are for structured mesh)

Table 4.4: Abaqus Results for CAX8RT element

Case No.	No. of Elements	Comp. Time (hr:min:sec)	Necking Start Radius (mm)	Final Rad. (mm)	Necking Start Time (mm)	Final Tempe. (^{o}C).
1	24	00:01:44	5.811	3.073	4.001	114.0
2	50	00:03:02.	6.050	2.771	4.000	114.5
3	100	00:03:26	6.066	2.691	3.342	115.0
4	200	00:05:08	6.072	2.553	3.612	116.0
5	400	01:08:53	6.072	2.292	3.75	116.0

[b)](All the values 2nd order structured mesh)

Table 4.5: Abaqus results for CAX6MT

Case No.	No. of Elements	Comp. Time (hr:min:sec)	Necking Start Radius (mm)	Final Rad. (mm)	Necking Start Time (mm)	Final Tempe. (^{o}C).
1	24	00:02:11	5.910	3.097	4.000	114.5
2	50	00:03:05	6.060	2.913	3.893	114.5
3	100	00:04:27	6.083	2.826	3.754	115.0
4	200	00:05:42	6.179	2.921	3.643	115.0
5	400	01:10:49	6.287	2.827	3.667	115.5

[c)](All the values are for 2nd order)

Chapter 5

Results from Academic Code

5.1 Introduction

The academic code is developed by Prof. Dr. Laurent STAINIER at Ecole Centrale de Nantes and Institute GeM. It consist of separate files for material, mesh, and python script. All these files were put on interaction with the help of gmsh in linux system. The results were taken by investigating the mesh parameters, material, and some other parameters.

5.2 Gmsh and Academic Code Files

Gmsh is open source code used for geometrical modeling and mesh generation with, initially developed by Christophe Geuzaine and Jean-François Remacle. The gmsh is developed as a fast, light and user-friendly software to easily create geometries and meshes that could be used in three-dimensional finite element solvers, and then visualize and export the computational results with maximum flexibility. There are also other open-source softwares available combining a CAD engine, a mesh generator and a post-processor, but the gmsh is mostly used among academic community, because of its easy availability and no charges, capability to integrate other software files and CAD capacity for all dimensions, and good post processing abilities. Gmsh however is unique in its design: It consist of a very small kernel with four modules, geometry, mesh, solver and post-processing, not tied to any particular computational solver, and designed to be driven both using a user-friendly graphical interface (GUI) and its own scripting language.

Each module can be controlled either interactively using the GUI or using the scripting language. The design of all four modules relies on a simple philosophybe fast, light and user-friendly.
Fast like, on a standard personal computer at any given point in time Gmsh should launch instantaneously, be able to generate a larger than aver- age mesh (compared to the standards of the finite element community; say, one million tetrahedron in 2008) in less than a minute, and be able to visualize such a mesh together with associated post-processing datasets at

interactive speeds.
Light like, the memory footprint of the application should be minimal and the source code should be small enough so that a single developer can understand it. Installing or running the software does not depend on any non-widely available third-party software package.
User-friendly, like the graphical user interface is designed in such a way that a new user can create simple meshes in a matter of minutes. In addition, the code is robust, portable, scriptable, extensible and thoroughly documented,all features contributing to a user-friendly experience.

The Url, http://www.geuz.org/gmsh/doc/texinfo/gmsh.html can be consulted for further information on gmsh. The link contains a free information, and is very useful for students interested in creating their own mesh and post-processing. The above passages of text have been excerpted from [33].

5.3 Test cases for quadrilateral and triangular elements

Here in the current chapter, the results of force, displacements, temperature, stress-strain curves and necking radius are explained with varying mesh sizes, element types and varying span of load application in some cases.

Case 1 The first case deals with the mesh of quadrilaterals of order one, with 12 elements each the necking zone and the zone without necking. The same mesh size is done with the triangular elements of order two. The values are noted separately in the tables listed below. The details and the graphs are shown respectively below.

Case 2 In the second case the mesh is of quadrilateral elements of order one, with 25 elements in both the necking zone and the zone without necking. The same mesh size is tested with the triangular elements of order two. The details and the graphs are shown respectively in the following.

Case 3 Here we have the quadrilaterals of order one, with 50 elements in both the necking zone and the zone without necking. The same mesh size is analyzed for triangular elements of order two. The details and the graphs are shown respectively in the following.

Case 4 This case deals with the mesh of quadrilaterals of order one, with 100 elements in both the necking zone and the zone without necking. The same mesh size is done for the triangular elements of order two. The details and the graphs are shown respectively in the following.

Case 5 The 5th case deals with the mesh of quadrilaterals of order one, with 200 elements in both the necking zone and the zone without necking. The same mesh size is simulated with the triangular elements of order two. The details and the graphs are shown respectively in the following.

Table 5.1: Quadrilateral Elements with Different Mesh Sizes

Case No.	No. of Elements	Comp. Time (hr:min:sec)	Necking Start Radius (mm)	Final Rad. (mm)	Necking Start Time (mm)	Final Tempe. (^{o}C).
1	24	00:02:19	5.913	3.063	4.25	111.50
2	50	00:04:39.	6.012	2.813	4.20	112.0
3	100	00:14:15	6.013	2.513	4.20	113.0
4	200	00:17:40	6.013	2.413	4.10	114.5
5	400	01:36:41	6.013	2.313	4.10	115.0

[a)](All the values are for 1st order)

Table 5.2: Triangular Elements with Different Mesh Sizes

Case No.	No. of Elements	Comp. Time (hr:min:sec)	Necking Start Radius (mm)	Final Rad. (mm)	Necking Start Time (mm)	Final Tempe. (^{o}C).
1	24	00:01:12	5.813	3.613	4.2	93.50
2	50	00:02:38.	5.913	3.013	4.2	100.0
3	100	00:05:53	6.013	2.813	4.2	102.5
4	200	00:15:37	6.013	2.413	4.1	113.5
5	400	01:51:56	6.013	2.410	4.1	114.5

[b)]All the values are for 2nd order

The results obtained in case of quadrilateral elements for academic code is given the table [5.1]. It is for the first order quadrilateral elements. The second order can not be executed in academic code. Similarly the results obtained for second order triangular elements is given in table [5.2]. The green line represents the first order quadrilateral elements while the red-brown line represents second order triangular elements. Here in academic code, the first order triangular elements (Constant strain triangular elements) show unstable behavior.

Necking radius for Abaqus and Academic code is also compared in the Figure [5.1], both for quadrilateral and triangular elements. The necking radius converges after the mesh size of 400 elements in both the cases.

The Figure:[5.2] represents the computational time variations and temperature variations for different number of elements. As usual the green line is for Abaqus result and the reddish brown shows the academic code. The first of Figure [5.2] are quadrilateral elements, it shows the high increase of computational time for academic code. While the second graph of Figure [5.2] are the triangular elements, the academic code starts the temperature variation from 95, and then it converge with Abaqus simulation for higher number of elements, but at the cost of high computational time.

The start of necking time for academic code is shown in the Figure [5.3]. Necking start earlier in the case of quadrilateral element as compared to triangular elements, and it converge for larger number of elements. The Figure [5.4] represents the first order and second

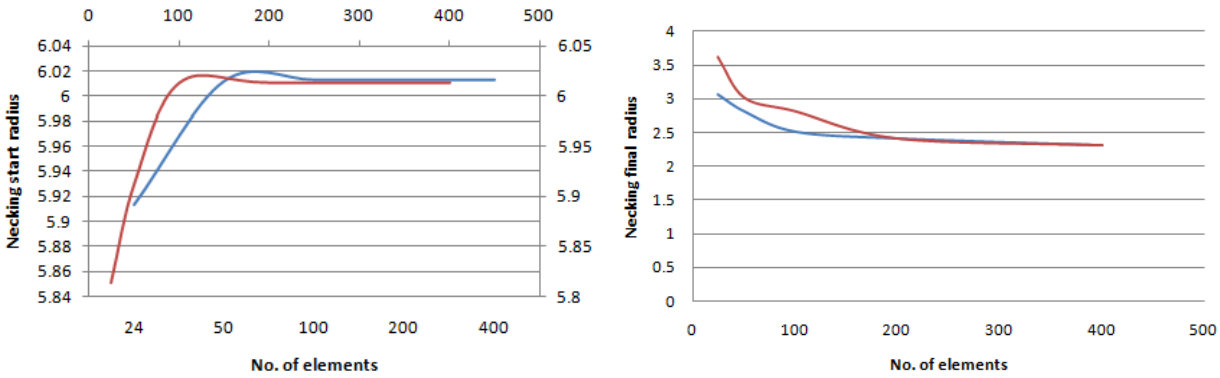

(a) Radius when the necking starts

(b) Radius when the necking ends

Figure 5.1: Radius variation for quadrilateral and triangular elements

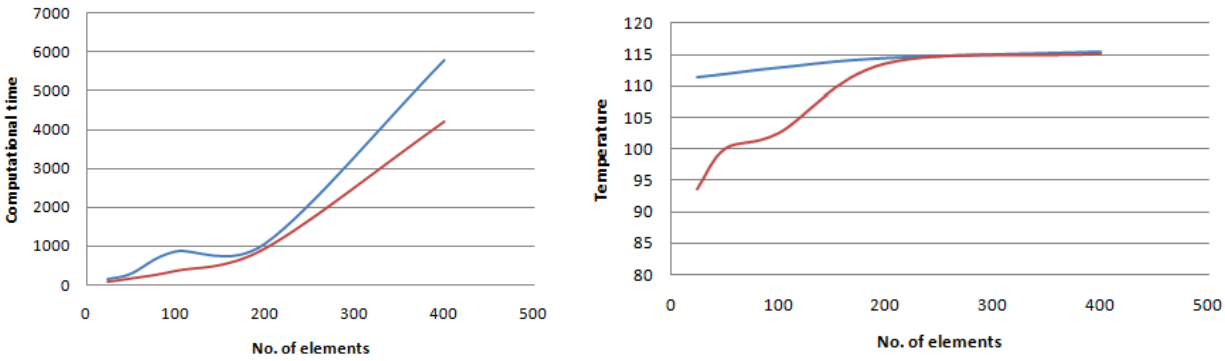

(a) Computational time variation

(b) Temperature variation

Figure 5.2: Academic Code: Quadrilateral and triangular element

order quadrilateral elements simulated in Abaqus. The results shows that the computational time in Abaqus is less than that of Academic code. For 400 elements and 800 elements, the computational time play a key role. For Abaqus, it is much less than the computational time for academic code. The green line represents the first order and the reddish line represents the second order quadrilateral elements. In the graph on the right, there is comparison of second order quadrilateral elements with the second order triangular elements in Abaqus. It is clear that for the second order quadrilateral elements the computational time is more than that of for second order triangular elements. The reason is the more number of integration points on the quadrilateral elements.

Here in the graph [5.5], the comparison of the computational time is given. The green line represents the Abaqus simulation and the reddish brown line represents the Academic code simulation. It is clear that the Abaqus is more takes less time for the simulation. But there are some difficulties with the some of the sections in Abaqus, e.g. during the interaction module and during the time-step module. The slight variation of the time changes the

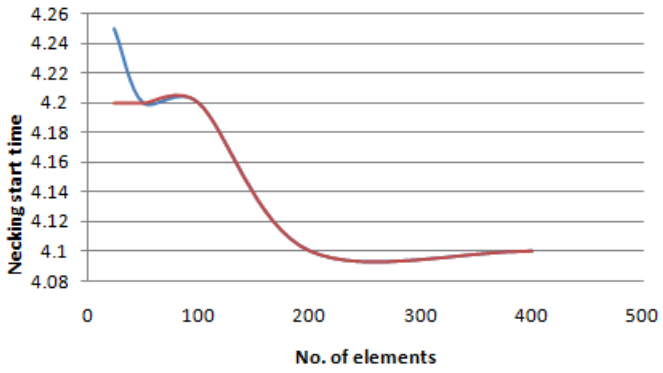

Figure 5.3: Necking start time: Quadrilateral and triangular element

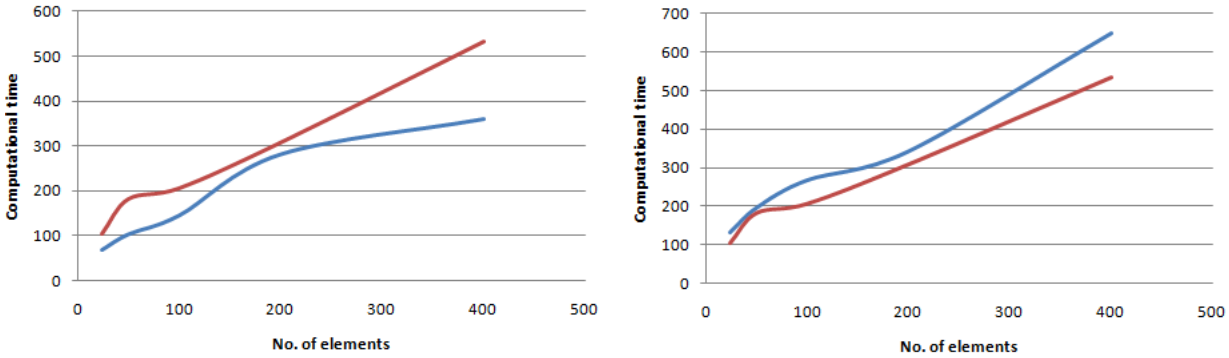

(a) 1st and 2nd order quadrilateral elements (b) 2nd order quadrilateral and triangular elements

Figure 5.4: Abaqus: Computational time for elements of first order and second order

solution a lot and as result the necking starts at different locations.

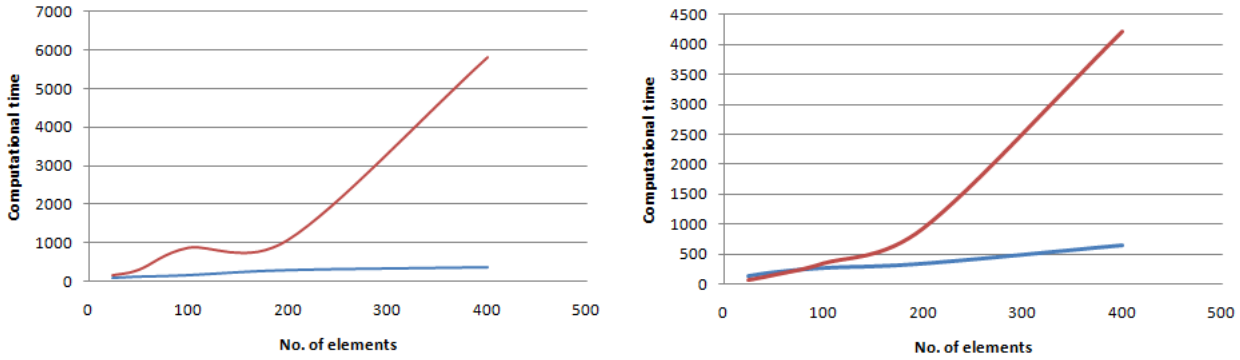

(a) 1st order quadrilateral elements (b) 2nd order triangular elements

Figure 5.5: Abaqus and Academic Code: Computational time

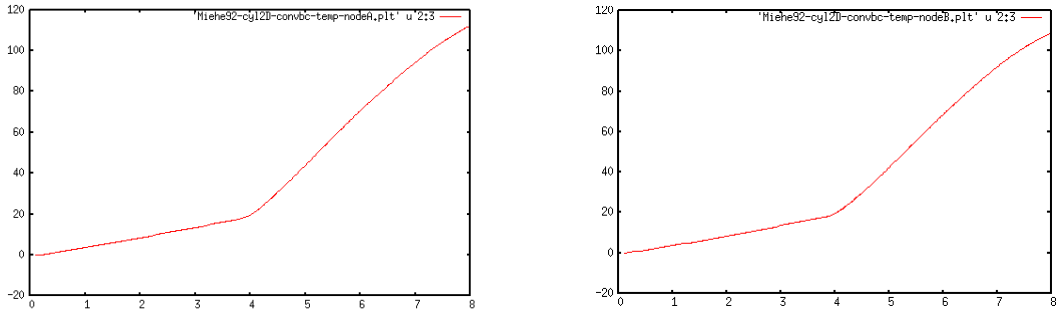

(a) Temperature on Inside element (b) Temperature on Outside element

Figure 5.6: Academic Code, Temperature-time variation

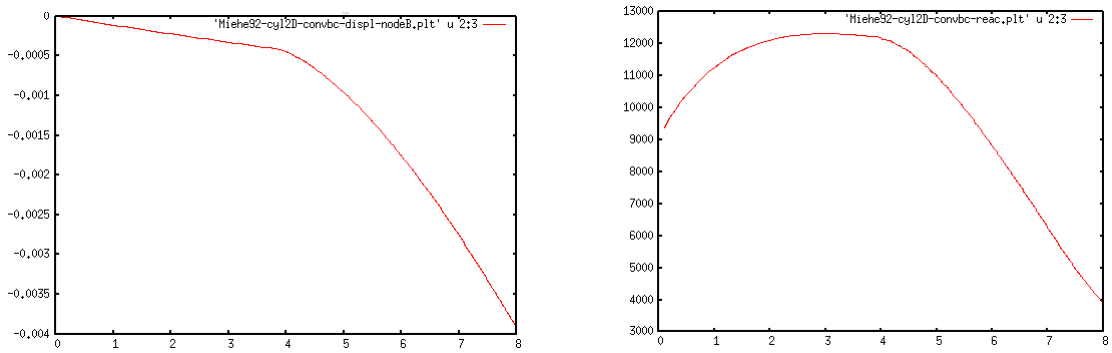

(a) Displacement of Outside element (b) Load-time Graph

Figure 5.7: Academic Code, Displacement and Load variation

Conclusion:

First of all, as advised by the professor, the reference papers in context of thermoplasticity and especially the tensile necking problem was studied. After getting the idea of thermoplastic constitutive models, the model was built in Abaqus, and in gmsh, in order to compare the Abaqus results with the results of reference paper results and with the academic code developed by Prof. Dr. Laurnt Stainiere ECN.

It worth to mention the different strain measures that one can get through Abaqus Post-processing facilities. There are various measures of strains which are mentioned in Appendix A. Besides numerous number of strain types, each element has different strain values according to the geometrical location of elements. So, the stress-strain graph need much care.

Although the temperature variation at normal temperature and constant material properties has very less variation with mesh size and other numerical parameters , but the numerical model of Abaqus was tested with temperature-dependent material properties, the same behavior was observed, with negligible variation, which is contrary to the results by, [29]. The numerical model can be further studied for such changes.

As for as the model by *Simo and Miehe* [13] is concerned, the model is formulated only for isotropic material. The kinematic hardening is not considered, as well the elastic thermal heat generation is also neglected. So, the kinematic relations of the model can be revised in future and formulated for both kinematic and isotropic hardening as well as for isomorphism, [30].
Similarly, the numerical formulation in Abaqus has shown unexpected result for convection heat coefficient. The convection heat coefficient was increased more than three times of the original, as was taken in *Simo and Miehe* [13], but the effect was observed as negligible. It can be investigated further upon taking the dependence of material properties on temperature.

Most important observation was the computational time, which was observed to be converged in case of Abaqus much earlier than the computational time observed in the academic code for the same mesh size. Among all of them, the most important was the time increment, which can result in a very long calculation with no results. At the end, the necking may occur at different location after simulation of 800 elements due to unsuitable time increment.

It is the time increment that define the strain rate and hardening, consequently, the plastic heat dissipation varies and it results in unstability.

As the necking starts at almost the same time in the current model, but it shows changes in varying the mesh types, especially the type of geometry of elements, but the overall behavior does not vary the results much. For triangular elements, it shows variation in Abaqus simulations for mesh size, but in academic code, these variations are negligible.

Appendix A

Strain Measure Types: The measurement options of strain results in the thermally triggered necking problem are given in the following.

1. **Integration Points:** At integration points , we can get the following results.
   (a) AC Yield (Active Yield Flag)
   (b) HFL (Heat Flux vector)
      i. Magnitude
      ii. HFL1
      iii. HFL2
   (c) LE (Logrithmic Strain Components)
      i. Max In-plane Principle
      ii. Min In-plane Principle
      iii. Out-of-plane Principle
      iv. Max Principle
      v. Mid Principle
      vi. Min Principle
      vii. LE11
      viii. LE22
      ix. LE33
      x. LE12
   (d) PE (Plastic Strain Components)
   (e) PEEQ (Equivalent Plastic Strain Components)
   (f) PEMAG (Magnitude of Plastic Strain)
   (g) S (Stress Components)
      i. Mises
      ii. Max In-plane Principle
      iii. Min In-plane Principle

iv. Out-of-plane Principle
v. Max Principle
vi. Mid Principle
vii. Min Principle
viii. Tresca
ix. Pressure
x. Third Invariant
xi. S11
xii. S22
xiii. S33
xiv. S12

2. **Centroid:** The same results as mentioned for Integration Points can be obtained for the Centoidal Points.

3. **Element nodal:** Same results can be obtained at each node of element but now for nodes istead of integration point and centoids.

4. **Unique nodal:** At the Unique nodal points, we have the same results with some extra results of force, temperature, point load, and temperature.

   (a) CF (Point loads)
      i. Magnitude
      ii. CF1
      iii. CF2

   (b) RF (Reaction force)
      i. Magnitude
      ii. RF1
      iii. RF2

   (c) U (Spatial displacement)
      i. Magnitude
      ii. U1
      iii. U2

   (d) RFL11 (Reaction Fluxes)

5. **Whole element** In the current thesis, there are no results to get for whole element.

6. **Surface face nodal:** As the case here is axisymmetric, the surface face nodal values are not important for the current case.

7. **Element face:** The element face can be taken in the list of post processing file data, but here we do not the element face results.

Weak form With the help of virtual strain, elastic stress-strain law and symmetricity of σ_{ij}, we get the weak form of the Principle of virtual work as follow.

$$\int_R C_{ijkl}\frac{\partial u_k}{\partial x_l}\frac{\partial \delta v_i}{\delta x_j}dV - \int_R b_i \delta v_i dV_o - \int_{\partial_2 R} t_i^* \delta v_i dA = 0 \tag{A.1}$$

$$u_i^b = \sum_{a=1}^{n} N^a(x^b) u_i^a \tag{A.2}$$

$$\delta v_i(x) = \sum_{a=1}^{n} N^a(x)\delta v_i^a \tag{A.3}$$

Substituting these interpolated values into the weak form, we get the equation:

$$\int_R C_{ijkl}\frac{\partial N^b(x)}{\partial x_l}u_k^b\frac{\partial N^a(x)}{\delta x_j}\delta v_i^a dV - \int_R b_i N^a(x)\delta v_i^a dV - \int_{\partial_2 R} t_i^* N^a(x)\delta v_i^a dA = 0 \tag{A.4}$$

Writing in the matrix form,

$$(K_{aibk}u_k^b - F_i^a)\delta v_i^a = 0 \tag{A.5}$$

where

$$K_{aibk} = \int_R C_{ijkl}\frac{\partial N^a(x)}{\partial x_j}\frac{\partial N^b(x)}{\delta x_l}\delta v_i^a dV \tag{A.6a}$$

$$F_i^a = \int_R b_i N^a(x)dV - \int_{\partial_2 R} t_i^* N^a(x)dA \tag{A.6b}$$

So due to Principle of virtual work we get the stress equilibrium equations in the form of integrals instead of differential equations. The integral equations are easy to handle. The Principle of virtual work is same as principle of minimun potential energy, but this is more easy to extend to non-linear problems and large shape changes.

Hyperelasticity; Equivalent principle virtual work equation: This equation now includes the deformation gradient and tangent stiffness for neo-Hookean materials.

$$\int_{V_0} \tau_{ij}\Big(F_{pq}({u_k}^b)\Big)\frac{\partial N^a}{\partial x_m}{F_{mj}}^{-1}dV_0 - \int_{V_0}\rho_0 b_i N^a dV_0 - \int_{\partial V_0} {t_i}^*\eta dA_0 = 0 \tag{A.7}$$

The stiffness matrix and reaction force force matrix for hyperelasticity can be written as;

$$K_{aibk} = \int_{V_0} C^e_{ijkl}\frac{\partial N^a}{\partial y_j}\frac{\partial N^b}{\partial y_l}dV_0 - \int_{V_0}\tau_{ij}\frac{\partial N^a}{\partial y_k}\frac{\partial N^b}{\partial y_j}dV_0 - \int_{\partial_2 R} t_i^* N^a(x)\frac{\partial \eta}{\partial {w^b}_k}dA_0 \tag{A.8}$$

$$R_i^a = \int_{V_0}\tau_{ij}\frac{\partial N^a}{\partial y_j}dV_0 \tag{A.9}$$

Bibliography

[1] J.C. Simo and T.J.R. Hughes, *Computational Inelasticity*, Springer-Verlag New York Inc. ISBN-13: 978-0387975207 (2006).

[2] Lemaitre J., Chaboch J.L., *Mechanics of Solid Materials*, Springer-Verlag New York Inc. ISBN-13: 978-0387975207 (2006).

[3] EA de Souza Neto, D. Peric, D.R.J Owen, *Computational Methods for Plasticity, Theory and Applications*, John Wiley and Sons, ISBN, 978-0-470-69452-7, (2008).

[4] O.C. Zienkiewicz, R. L. Taylor, J. Z. Zhu, *The Finite Element Method, its Basis and Fundametals*, 6th Edition Elsevier.

[5] J. Chakrabarty, *Theory of Plasticity*, 3rd Edition Elsvier.

[6] R. Hill, *The Mathematical Theory of Plasticity*, Clarendon Press Oxford, 1950.

[7] K. Washizu, *Variational Methods in Elasticity and Plasticity*, 3rd Edition Pergamon.

[8] R. D. Cook, *Finite Element Modeling for Stress Analysis*, John Wiley and Sons, Inc., Chichester, 1995. ISBN 0-471-11598-3.

[9] E. Hinton, D. R. J. Owen, *Finite Element Programming*, Pinerdge Press, Swansea, (1997), ISBN 0-12-349359-1.

[10] B.D. Coleman and M.E. Gurtin, *Thermodynamics with internal state variables*, J. Chem. Phy. 47(1967) 597-613

[11] F. Armero and J. C. Simo, *A priori stability estimates and unconditionally stable product formula algorithms for nonlinear coupled thermo-plasticity*, International Journal of Plasticity, Vol.**9**, 749-782, 1993.

[12] F. Armero and J.C. Simo, *A new unconditionally stable fractional step method for nonlinear coupled thermo-mechanical problems*, International Journal for Numerical Methods in Engineering, Vol. **35**, 737-766 (1992).

[13] J.C. Simo and C. Miehe, *Associative Coupled Thermoplasticity at Finite Strains: Formulation, Numerical Ananlysis and Implementation*, Computer Methods in Appl. Mech. and Engg. **98** (1992) 41-104.

[14] Q. Yang, L. Stainier, M. Ortiz, *A variational formulation of the coupled thermo-mechanical boundary value problem for general dissipative solids*, Journal of the Mech. and Phy. of Solids, **54** (2006), 401-424.

[15] Stainier, L., and M. Ortiz, *Study and validation of variation theory of thermo-mechanical coupling in finite visc-plasticity*, Inter. Jr. of Solids and Structures, **47** (2010) 705-715.

[16] P. Wriggers, C. Miehe, M. Kleiber, J. C. Simo, *On the coupled thermo-mechanical treatment of necking problems via finite element methods*, Inter. Jr. of Numerical Methods in Engineering, Vol. **33**, 869-883 (1992).

[17] J. H. Argyris and J. S. Doltsinis, *On the large strain inelastic analysis in natural formulation, Part 1*, Comp. Methods Appl. Mech. Eng., **20**, 213-252 (1979).

[18] J. H. Argyris and J. S. Doltsinis, *On the natural formulation and analysis of large deformation coupled thermo- mechanical problems*, Comp. Methods Appl. Mech. Eng., **25**, 195-253 (1981).

[19] J. H. Argyris, J. S. Doltsinis, P. M. Pimenta and H. Wiistenberg, Thermomechanical response of solids at high strains-Natural approach, Comp. Methods Appl. Mech. Eng., 32, 3-57 (1982).

[20] H. Balmer, J. S. Doltsinis and M. Konig, *Elastoplastic and creep analysis with ASKA program system*, Comp. Methods Appl. Mech. Eng., **3**, 87-104 (1974).

[21] W. H. Chen, *Necking of a bar*, Int. J . Solids Struct., 7 , 685-717 (1971).

[22] H. Ghoneim and S. Matsuoka, *Thermoviscoplasticity by finite element: Tensile and compression test*, Int. J . Solids Struct., **23**, 1133-1143 (1987).

[23] T. J. R. Hughes, *The Finite Element Method*, Prentice-Hall, Englewood Cliffs, N.J., 1987.

[24] Th. Lehmann.and U. Blix, *On the coupled thermo-mechanical process in the necking problem*, Int. J . Plhst., 1, 175-188 (1985).

[25] A. Needleman, *A numerical study of necking in circular cylindrical bars*, J . Mech. Phys. Solids, 20, 111-127 (1972).

[26] J. C. Simo, *A framework for finite strain elastoplasticity based on the multiplicative decomposition and hyperelastic relations. Part II: Computational aspects*, Comp. Methods Appl. Mech. Eng., 66, 1-31 (1988).

[27] J. C. Simo, *A framework for finite strain elastoplasticity based on maximum plastic dissipation and the multiplicative decomposition: Part I. Continuum formulation*, Comp. Methods Appl. Mech. Eng., 66, 199-219 (1988).

[28] T. J. R. Hughes, I. Levi and I. Winget, *An Element-by-element implicit algorithms for heat conduction*, J. Engg. Mech. **109(2)**(1983) 576-586.

[29] Marko Canadija and Josip Brnic, *Associative coupled thermoplasticity at finite strain with temperature-dependent material parameters*, International Journal of Plasticity 20 (2004) 18511874, (2003).

[30] A. Ibrahimbegovic and L. Chorfi, *Viscoplasticity model at finite deformations with combined isotropic and kinematic hardening*, Comput. Struct. 77, 509525,(2002).

[31] Armero, F., Simo, J.C., 1992. *A new unconditionally stable fractional step method for non-linear coupled thermomechanical problems*. Int. J. Numer. Meth. Eng. 35, 737766.

[32] Rosakis, P., Rosakis, A.J., Ravichandran, G., Hodowany, J., 2000, *A thermodynamic internal variable model for the partition of plastic work into heat and stored energy in metals.*, J. Mech. Phys. Solids 48, 581607.

[33] Christophe Geuzaine, Jean-François Remacle, *An introduction to geometrical modelling and mesh generation with Gmsh*, 2008.

[34] Dr. Sebastian Nervi, and Dr. Ricardo L. Actis, *Incremental Theory of Plasticity*; October, 2008.

[35] A. Bertram, *Finite thermoplasticity based on isomorphisms*, April, (Otto-von-Guericke-Universita 39106 Magdeburg, Germany), (2003).

[36] C. Truessdell and W. Noll, *The non-linear field theories of mechanics*, Springer, Berlin (1965).

Afterword

Not to mention more about plasticity, the author would like to applaud the comprehension and appreciation of the reader after the completion of the afore mentioned thesis. The idea of the current subject has initiation from the notable lectures of Dr. Laurent Stainier regarding the coupled problems. The lectures were given as a part of the Erasmus Mundus courses in May, 2010. The lectures were given in very delicate manners, a way the students can be instigated and incited to find the solutions by themself. That inspirations, I got from the lectures evoke me for the coupled problems in plasticity. I express my will and requested Dr. Laurent Stainier for the topic of thesis. I was lucky to have the topic and working in the supervision of Dr. Laurent Stainier at ECN Nantes, France. All the tasks of the thesis were accoplished with the remarkable support of Dr. STAINIER, L. and the enthusiastic community at Ecole Centrale Nantes.

Indeed no piece of literature can be completed without the commments of reader. The essence of my writings would be the worthy comments, questions and answers that a reader is concerned with. On behalf of my professor, and me, of course, the reader is encouraged to be confident while if he/she has any sort of question regarding the subject; I would feel good to answer the question as much as possible.

Shabeer Khan,
June, 2011.
Nantes, France.